Loss of Mitochondrial FMT Restores Chloroplast Proteostasis via Inter-organelle Compensation

Jitae Kim[1*], Changhee Na[2], Pratyush Routray[3], NoA Bae[1], Hanseul Kim[1], Jae-Yeon Kim[1], Da Been Kim[2], Namil Son[4], Zeeshan Nasim[5,6], Ryoung Lee[1], Ji Hyun Kang[2], Geoni Choi[2], Hyoungseok Lee[7], Ji Hoon Ahn[5], Byeong-ha Lee[1], Dong Wook Lee[2,8*], Klaas J. van Wijk[3*]

[1] Department of Life Science, Sogang University, Seoul, 04107, Republic of Korea.

[2] Department of Integrative Food, Bioscience and Biotechnology, Chonnam National University, Gwangju, 61186, Republic of Korea.

[3] Department of Plant Biology, Cornell University, Ithaca, New York 14853, USA.

[4] Department of Plant Sciences, University of Cambridge, Cambridge CB2 3EA, UK.

[5] Department of Life Sciences, Korea University, Seoul 02841, Republic of Korea.

[6] Department of Applied Plant Science, Chonnam National University, Gwangju, 61186, Republic of Korea.

[7] Division of Life Sciences, Korea Polar Research Institute, Incheon, 21990, Republic of Korea.

[8] Department of Bioenergy Science and Technology, Chonnam National University, Gwangju, 61186, Republic of Korea.

* Authors for correspondence: jkim222@sogang.ac.kr (J.K.), ldw4844@jnu.ac.kr (D.W.L.), kv35@cornell.edu (K.J.v.W.)

ABSTRACT

Chloroplast proteostasis is vital for plant development, yet how cells recover chloroplast function when essential components of the plastid protease system fail remains unclear. Here, using a forward genetic suppressor screen in Arabidopsis, we identify loss of the mitochondrial protein FRIENDLY MITOCHONDRIA (FMT) as a strong suppressor of the virescent and small *clpc1* mutant, which lacks the chloroplast Clp protease chaperone ClpC1. Suppression is mediated by transcriptional upregulation of *CLPC2*, a ClpC1 paralog, enabling functional compensation. RNA sequencing and quantitative comparative proteomics reveal coordinated remodeling of nuclear gene expression and chloroplast protein investment, including recovery of photosynthesis-associated proteins and attenuation of plastid stress-associated signatures in *fmtclpc1*. Genetic analyses further show that REC family proteins are required for full *CLPC2* upregulation and associated phenotypic recovery. Together, these findings reveal a latent capacity for inter-organelle compensation that can restore chloroplast proteostasis when ClpC1 function is compromised.

INTRODUCTION

Plant survival depends on the ability of its energy-producing organelles to communicate and maintain proteostasis despite continual developmental, metabolic, and environmental fluctuations [1,2]. Chloroplasts and mitochondria rely on thousands of nuclear-encoded proteins that must be precisely synthesized, imported, and folded, rendering both organelles acutely vulnerable to even modest disruptions in protein homeostasis [3,4]. Because failures in these processes compromise photosynthesis, metabolism, and growth, plants must deploy coordinated cellular responses to proteotoxic stress across organelles [5-7]. Yet how such organelle dysfunction is integrated at the cellular level, and in particular how chloroplast function can recover when essential components of its proteostasis machinery fail, remains largely unknown.

In chloroplasts, proteostasis relies heavily on the stromal Clp chaperone–protease system, the most abundant and broadly acting proteolytic machinery in the organelle [8,9]. The ClpPR core comprises catalytically active ClpP1 and ClpP3–6 and non-enzymatic ClpR1–4 subunits arranged as two stacked heptameric rings [10-13]. Substrate unfolding and translocation are mediated by the AAA+ chaperones ClpC1, ClpC2, and ClpD, while accessory proteins such as ClpT1/2, ClpS1, and ClpF contribute to core assembly/stabilization and substrate selection [14-17]. The turnover of numerous stromal proteins—including the canonical substrate PAA2/HMA8, a copper transporter in the thylakoid—highlights the central role of the Clp machinery in chloroplast protein quality control [18].

ClpC1 is a pivotal component of this system. It functions both as the major unfoldase that delivers substrates to the ClpPR core [19] and is also involved in quality control of imported proteins at the inner envelope membrane [20]. Loss of ClpC1 leads to severe chloroplast dysfunction, manifesting as chlorosis, impaired photosynthesis, and markedly reduced growth. Protein-import stress is a known trigger of retrograde transcriptional reprogramming [21], and recent work has shown that GUN1 directly binds and stabilizes a subset of plastid RNAs, identifying plastid RNA maturation as a key upstream determinant of plastid-to-nucleus signaling [22]. Despite these advances, it remains unclear whether plants possess intrinsic recovery pathways capable of re-establishing chloroplast proteostasis when a core chaperone such as ClpC1 is lacking.

Mitochondria also undergo dynamic structural and functional remodeling in response to stress [23-25]. The conserved CLU-family protein FRIENDLY MITOCHONDRIA (FMT) maintains mitochondrial distribution, dynamics, and homeostasis; *fmt* mutants exhibit clustered mitochondria, altered organelle contacts, elevated ROS, and growth defects [26,27]. FMT associates with cytosolic ribosomes at the mitochondrial surface to promote translation of nuclear-encoded mitochondrial mRNAs [28,29], and contributes to mitophagy during de-etiolation [30], but no role has been identified for FMT in plastid communication or proteostasis. Arabidopsis encodes three FMT-related homologues—*REC1-3*—that regulate chloroplast compartment size, and in tomato they additionally influence plastid development and plastid-related gene expression [31,32], although their functions in organelle stress responses remain unresolved.

To identify pathways capable of actively restoring chloroplast proteostasis when ClpC1 function is lost, we performed a forward EMS suppressor screen in the severe chlorotic *clpc1-1* mutant. Multiple independent suppressors carried mutations in *FMT*, revealing an unexpected connection between mitochondrial perturbation and recovery of chloroplast function. RNA-seq analysis and comparative proteomics revealed coordinated remodeling of nuclear gene expression and chloroplast protein investment, consistent with a distributed compensatory response. We show that loss of *FMT* is associated with increased *REC2* expression and transcriptional upregulation of *CLPC2,* a ClpC1 paralog, and that *REC1* and *REC2* are required for full *fmt*-mediated compensation. Elevated ClpC2 functionally substitutes for ClpC1, restoring chloroplast proteostasis, pigmentation, and growth. Together, these findings uncover an inter-organelle compensatory mechanism that restores chloroplast proteostasis when ClpC1 function is compromised.

RESULTS

Suppressor screen and WGS identify *FMT* mutations

To identify new genetic factors involved in chloroplast proteostasis and gain insight into cellular responses to ClpC1 deficiency, we performed a forward EMS suppressor screen in the *clpc1-1* background. Among ~10,000 mutagenized M2 seedlings, we recovered multiple individuals exhibiting restored greening and enhanced growth, and four of the strongest suppressor lines were selected for detailed analysis (Fig. 1A,B). Bulked segregant whole-genome sequencing mapped all four suppressors to *FMT* (At3g52140), each carrying a distinct EMS-induced lesion affecting coding sequence or splice sites (Fig. 1C; Supplementary Table 1). These independent mutations were consistently associated with substantial phenotypic recovery in the *clpc1-1* background (Fig. 1B).

Genetic analyses confirm *FMT* as the causal suppressor

To test whether loss of *FMT* is responsible for suppression, we reintroduced a genomic *pFMT::FMT* construct into each EMS-derived line, which restored the characteristic chlorotic *clpc1-1* phenotype (Fig. 1D). Two independent T-DNA insertion alleles, *fmt-3* and *fmt-4*, similarly suppressed *clpc1-1* as double mutants (Fig. 1E). Semi-quantitative RT–PCR confirmed reduced or mis-spliced *FMT* transcripts across EMS alleles, severe transcript reduction in *fmt-3*, and loss of C-terminal amplicons in *fmt-4*. *CLPC1* transcripts remained absent in all *clpc1-1* backgrounds, while *FMT* was elevated in *clpc1-1* relative to wild type (Supplementary Figure 1). Heteroallelic crosses further supported allelism: F1 progeny from *fmt-3clpc1-1* × *fmt-4clpc1-1* and from each EMS-derived *socc-clpc1-1* × *fmt-3clpc1-1* cross displayed the same suppressed phenotype (Supplementary Figure 2A), establishing that all *socc* alleles represent loss-of-function mutations in *FMT*.

CRISPR tests validate that suppression reflects true interaction with *CLPC1*

To rule out T-DNA–specific artifacts of the *clpc1-1* allele, we generated two CRISPR-derived *clpc1* null alleles (*clpc1-4*, *clpc1-5*), each carrying frameshift mutations in exon 4. Both alleles phenocopied *clpc1-1* and failed to complement it in heteroallelic crosses (Supplementary Figure 2B). Importantly, both were robustly suppressed by *fmt-3* (Fig. 1G), demonstrating that *fmt*-mediated rescue reflects a true genetic interaction with *CLPC1* rather than epigenetic reactivation [33,34] of the T-DNA insertion. Consistent with this genetic recovery, *fmt* suppressors exhibited substantially higher Fv/Fm and pigment levels relative to *clpc1-1*, approaching wild-type values (Fig. 1F). Together, these results establish *FMT* loss of function as the causal basis of all recovered EMS suppressors and demonstrate that disruption of *FMT* restores chloroplast performance in *clpc1-1* through a genuine genetic interaction with *CLPC1*.

fmt specifically suppresses *clpc1-1* but not other chloroplast Clp components or protein import mutants

To test the specificity of *fmt*-mediated suppression on the Clp system, we examined genetic interactions between *fmt* and mutants affecting other components of the chloroplast Clp system. Neither *fmt-3* nor *fmt-4* suppressed the pale, small phenotype of *clpr2-1* [35] (Fig. 2A), and *fmt-4* failed to rescue the severe developmental defects of the *clpt1-2clpt2-1* [15] double mutant (Fig. 2B), indicating that *fmt* does not bypass defects in the Clp protease complex.

We next tested whether *fmt* affects chloroplast protein import. Introducing *fmt-3* into the TOC33 and TIC40 mutants *ppi1-1* [36] and *tic40-4* [37] yielded smaller and more chlorotic double mutants than either single mutant (Fig. 2C,D). These results show that *fmt* does not restore defects in chloroplast protein import and that loss of FMT further impairs plastid function when import is compromised. Thus, *fmt* suppression is highly specific to *clpc1-1* and does not reflect general rescue of Clp or import defects.

fmt-mediated suppression of *clpc1-1* operates independently of *GUN1*

To examine whether *fmt* interacts with plastid-to-nucleus retrograde signaling pathways [21], we combined *fmt* alleles with *gun1-101*. While *fmt* and *gun1-101* single mutants were uniformly green, all *fmtgun1-101* double mutants displayed a distinctive variegated phenotype (Fig. 2E), indicating that loss of *GUN1* results in unstable chloroplast biogenesis and function in *fmt* backgrounds. Despite this combinatorial (or synergistic) effect of *gun1* and *fmt*, *fmt* was still able to suppress the reduced plant growth and virescent phenotype of *clpc1-1* in the absence of *GUN1,* as observed in *fmt-3*, *fmt-4*, and *socc20-1* backgrounds (Fig. 2F). However, the triple mutants retained the variegation characteristic of *fmtgun1-101,* indicating that loss of ClpC1 and loss of GUN1 have different underlying molecular causes (Fig. 2F).

fmt restores chloroplast ultrastructure and ClpC1-dependent proteostasis

To understand how *fmt* suppresses the *clpc1-1* phenotype, we examined chloroplast ultrastructure and proteostasis. *clpc1-1* chloroplasts were swollen with reduced stromal density and poorly stacked thylakoids, whereas *fmt-3clpc1-1* double mutants displayed compact chloroplasts with dense stroma and well-organized grana, closely resembling wild type despite retaining the characteristic mitochondrial clustering of *fmt* (Fig. 3A). We next examined the protein levels of the Clp substrate adaptors ClpF, ClpS1 and the established Clp substrate PAA2, a copper transporter in the thylakoid membrane [18]. Immunoblotting showed that *clpc1-1* accumulated high levels of ClpF, ClpS1, and the ClpC1 substrate PAA2 (Fig. 3B), consistent with previous reports [14,17,18]. In *fmt-4clpc1-1* and *socc20-1clpc1-1*, ClpS1 and PAA2 levels decreased toward wild-type abundance, and ClpF levels trended downward. To directly assess proteolytic activity, we performed a Cu^{2+}-dependent PAA2 degradation assay [18] (Fig. 3C). PAA2 turnover—impaired in *clpc1-1*—was restored in all *fmt* suppressors but not in *fmt-3clpr2-1*, indicating that *fmt* specifically rescues the loss of ClpC capacity but not loss of Clp protease complex capacity.

fmt induces *CLPC2*, and native promoter–driven *CLPC2* elevation is sufficient for rescue of *clpc1-1*

Because the close homolog ClpC2 can compensate for ClpC1 when expressed at higher levels [38], we quantified *CLPC2* and *CLPD* transcripts. All *fmt* and *fmtclpc1-1* lines showed an approximately twofold increase in *CLPC2*, while the more distant *CLPD* chaperone (~50% sequence identity to ClpC1 and ClpC2) remained largely unchanged (Fig. 3D), indicating that loss of *FMT* selectively induces *CLPC2*. To test whether this induction is sufficient for *clpc1-1* suppression, we expressed genomic *CLPC2* under its native promoter in *clpc1-1*. These lines showed 2-4-fold increases in *CLPC2* transcripts compared with *clpc1-1* and displayed proportional rescue of greening and pigment accumulation (Fig. 3E–G) (*i.e.* higher *CLPC2* transcript levels result in better suppression/complementation), demonstrating that a several-fold increase in ClpC2 is enough to offset complete loss of *clpc1-1*. The scaling of *CLPC2* expression across the overexpression lines is consistent with differences in *gCLPC2* copy number, and indicates that the promoter is not saturated in the *clpc1-1* background.

FMT overexpression represses *CLPC2* and exacerbates *clpc1-1*

To examine the relationship between *FMT* and *CLPC1*, *FMT* was overexpressed under its native promoter in the *clpc1-1* background. These lines exhibited chlorotic phenotypes of different severity, inversely correlated with *FMT* expression (Supplementary Figure 3A–C). The strongest overexpression lines closely resembled the *clpc1-1clpc2-2* double mutant, although they were slightly larger in size (Fig. 3H). These lines showed reduced *CLPC2* transcript levels that were intermediate between those of *clpc1-1* and *clpc1-1clpc2-2* (~60–70% of *clpc1-1*; Fig. 3D). Consistent with the severe chlorotic phenotype, total chlorophyll contents and Fv/Fm values were reduced in both the FMT overexpression lines and the *clpc1-1clpc2-2* mutant relative to *clpc1-1* (Fig. 3I).

RNA-seq reveals coordinated transcriptional remodeling associated with *clpc1* suppression

To better understand the molecular phenotypes of *fmt* and *clpc1-1,* and suppression of the *clpc1-1* phenotype in *fmtclpc1-1*, we performed RNA-seq analysis of Arabidopsis seedlings at developmental stage 1.07 for WT, *fmt-3, clpc1-1*, *fmt-3clpc1-1* and *FMT/clpc1-1 (OE#1).* After mapping, quality control, and normalization, mRNA expression values were obtained for 21,202 genes (Supplementary Data Set 1A), and pairwise differential expression statistics were calculated for downstream analyses. Principal Component Analysis (PCA) showed a very distinct signature for *clpc1,* which was further enhanced in *FMT*/*clpc1* (Fig. 4A). *fmtclpc1* was more closely related to WT, whereas *fmt* was very similar to WT but remained distinct from *fmtclpc1*. The PCA results are consistent with the observed phenotypes across these five genotypes.

We extracted all genes that showed a pairwise difference of at least 2-fold (x<0.5 or x>2) with P<0.01 in at least one of the 10 possible comparisons across genotypes (Supplementary Data Set 1B). This resulted in 4,745 nuclear protein-coding genes that we annotated for subcellular protein location and function (Supplementary Data Set 1B). Gene cluster analysis showed three main clusters (I, II, III) that each further separated into three subclusters (Fig. 4B). Cluster I is dominated by genes for which the mRNA is enriched in *clpc1* and *FM*T/*clpc1* often with most enhanced expression in *FMT/clpc1*. Cluster II is enriched for genes that are reduced in *clpc1* and *FMT/clpc1*. Cluster III contains genes with mRNA generally enriched only in *fmtclpc1* as compared to the other four genotypes. MapMan [39] functional bin analysis shows that cluster I and III are both highly depleted for genes encoding photosynthetic proteins (Fig. 4C). Cluster I, but not clusters II and III, is also relatively low in genes involved in mitochondrial electron transport/ATP synthesis (bin 9), tetrapyrrole metabolism (bin 19) and amino acid metabolism (bin 13). Cluster I is most enriched for genes involved in DNA and RNA related processes. Most genes in cluster III (subcluster 8 and 9) are expressed much higher in *fmtclpc1* than in any of the other four genotypes; this cluster is especially enriched for signaling (bin 30) and stress (bin 20) (Fig. 4C). Figure 4D shows the bin-cluster analysis for the genes encoding experimentally confirmed plastid-, mitochondrial-, and dually localized proteins (556, 58 and 15 genes, respectively). 72% belong to cluster II. RNA metabolism shows strong enrichment for cluster I – many of these are PPR proteins with functions in editing and RNA processing of plastid- or mitochondria-encoded genes. Proteins involved in the protein life cycle (bin 29) are also enriched in this cluster I. Photosynthetic functions (bin 1) and starch metabolism (bin 2) are nearly exclusively in cluster II, consistent with the loss of photosynthesis phenotypes of *clpc1* and *FMT/clpc1*. In contrast, amino acid metabolism (bin 13), sulfur assimilation (bin 14), and hormone synthesis (bin 17 - nearly exclusively proteins involved in plastid jasmonate metabolism, including allene oxide cyclase 1, 2, 3, and 4; allene oxide synthase; and lipoxygenase 1 and 2) are enriched in cluster III.

Subcluster 4 (376 genes) stands out for its high mRNA levels in the *fmt* line compared to the other four genotypes. Many of the genes with the most pronounced expression profiles encode mitochondrial proteins (Supplementary Figure 4A), including alternative oxidase 1A (AOX1A), stomatin-like protein 2 (SLP2), heat shock protein HSP23.5, DUF295 domain protein DOB5, and external NAD(P)H dehydrogenase subunit B3 (NDH-B3), all of which are reported to have low basal expression levels [40]. AOX1A and NDH-B3 partially uncouple respiration from mitochondrial

ATP production and thereby reduce mitochondrial reactive oxygen species (ROS) production [41]. AOX1A is a marker of the mitochondrial retrograde response [42]. SLP2 affects protein abundance and activity of respiratory complex I, likely through effects on its assembly and/or stability [43,44]. HSP23.5 is a member of the HSP20-like chaperone superfamily; although this specific protein has not been characterized, mitochondrial HSP20 chaperones are important for facilitating protein folding within mitochondria, particularly under stress conditions [45]. DUF295 domain protein DOB5 has not been characterized but is part of the large DUF295 family [46]. Notably, subcluster 4 contains eight DUF295 family members, seven of which are predicted to encode mitochondrial proteins. Many mitochondrial DUF295 proteins are induced by mitochondrial dysfunction [46], which is highly consistent with their elevated abundance in the *fmt* background.

Subclusters eight and nine (within cluster III) contain genes with high mRNA levels in *fmtclpc1* compared to the other four genotypes. These genes may provide clues about the nature of *clpc1* suppression by *fmt.* Among the confirmed plastid and mitochondrial proteins, we identified five genes for which the RNA levels in *fmtclpc1* were more than threefold higher than in each of the other four genotypes (Supplementary Figure 4B). Surprisingly, all five are involved in jasmonate or salicylic acid metabolism or response; these include two allene oxide cyclases (AOC1 and AOC3) and lipoxygenase 3 involved in JA synthesis [47], the plastid envelope MATE transporter EDS5, which is likely involved in SA export from plastids [48], and mitochondrial arginase 2 (ARGAH2), which is highly induced by methyl jasmonate [49]. Furthermore, the plastid Sigma1 interacting factor (Sib1, At3g56710) [50] is also highly expressed in *fmtclpc1* compared to *clpc1* (6.3-fold) and 2-3 fold compared to WT and *fmt*. Sib1 has been shown to be involved in JA and SA responses either within the chloroplast or in the nucleus [51,52]. Overexpression of Sib1 causes hyperactivation of defense-related genes following SA and JA treatments [51]. These results suggest that JA and SA play an important role in the suppression of *clpc1* by *fmt.*

Some 30 transcription factors (TFs) have been highlighted as important during chloroplast and/or mitochondrial dysfunction, stress, retrograde signaling, or plastid biogenesis and proteostasis [42,47,53-55] (Supplementary Table 3). Fifteen of these TFs showed at least one pairwise differential expression (adj. $P<0.01$) (Supplementary Data Set 1B; Fig. 4B). Four of these—HSFA2, GLK1, BBX15, and WRKY40 (At2g26150, At2g20570, At1g25440 and At1g80840)—showed significant differential expression patterns consistent with contributing to *clpc1* suppression (Fig. 4E). HSFA2 (cluster II-4) was strongly upregulated in *fmt* compared to WT but reduced in *clpc1,* with partial restoration in *fmtclpc1.* Notably, HSFA2 was also elevated in the *FMT/clpc1* background despite a more chlorotic and smaller phenotype, indicating that HSFA2 induction does not correlate with phenotypic recovery and is unlikely to be a primary driver of *clpc1* suppression. In contrast, GLK1 (cluster II-6) was unaffected in *fmt* but strongly suppressed in *clpc1* and *FMT/clpc1,* with partial restoration in *fmtclpc1.* The zinc-finger TF BBX15 (cluster II-4) [56] was upregulated in *fmt* and downregulated in *clpc1* and *FMT/clpc1,* but restored to WT levels in *fmtclpc1*. WRKY40 (cluster III-9), which is involved in attenuation of basal pathogen defense and is upregulated by GLK1/2 [57], was elevated in *fmtclpc1,* likely reflecting a genetic interaction between *fmt* and *clpc1*. We note that the RNA levels of the well-studied TFs HY5 and GLK2 (both positive regulators of genes encoding chloroplast proteins involved in photosynthesis and chlorophyll synthesis), as well as the direct GLK1 target BBX14 (a homolog of BBX15)

implicated in chloroplast development [58], were not significantly different (adj. P<0.01) across these five genotypes.

Comparative proteomics reveals coordinated remodeling of chloroplast protein investment during *clpc1* suppression

To understand the suppression effect of *fmt* on the *clpc1* leaf proteome phenotype, total leaf proteomes of *clpc1-1* and *fmt-3clpc1-1* were compared by quantitative proteomics. A total of 2,975 proteins and protein groups comprising close homologs were identified, most of which (95%) were detected in both genotypes (Supplementary Data Set 2). Correlation analysis and principal component analysis (PCA) showed clear separation between genotypes and low variation among biological replicates (Supplementary Figure 5A,B). Of the identified proteins, 1,266 (43%) were localized to chloroplasts and/or mitochondria, representing ~65% of all matched spectra. The five thylakoid complexes involved in the light reactions (PSII, PSI, cytochrome b6f, NDH and ATP synthase) all increased between 32% and 49%, whereas the Calvin-Benson cycle enzymes collectively increased by 25% in *fmtclpc1* compared with *clpc1*, consistent with suppression of the virescent phenotype (Supplementary Figure 5C). Consequently, relative investment in most other functional categories decreased, except for gluconeogenesis/glyoxylate cycle (bin 6), nitrogen metabolism (bin 12), and the TCA cycle/organic acid metabolism (bin 8), which increased by 9%, 4% and 3%, respectively. The relative abundance of the chloroplast ClpPRT complex was slightly lower (18%), whereas ClpC2 was 36% higher in *fmtclpc1* compared with *clpc1-1* (ClpC1 was not detected) (Fig. 5A), consistent with increased *CLPC2* RNA levels (Fig. 3D).

Figure 5B shows the volcano plot of individual proteins comparing the two genotypes. At P<0.01 and a >2-fold difference between genotypes, 13 proteins increased and 32 decreased in *fmtclpc1* compared with *clpc1* (Fig. 5B,C). All 13 increased proteins were plastid (8) or mitochondrial (4), except for REDUCED CHLOROPLAST COVERAGE 2 (REC2), which is localized to the cytosol. REC2 was enriched 2.3-fold in the double mutant. REC2 has two homologs (REC1 and REC3), and the REC family is phylogenetically related to FMT. REC1 and REC3 were detected in both genotypes, whereas FMT was detected only in *clpc1-1* and not in *fmtclpc1-1*, consistent with *fmt* being a null line; REC1 and REC3 did not change significantly (Fig. 5D).

Six of the increased chloroplast proteins are directly involved in the light reactions of photosynthesis, consistent with suppression of the virescent *clpc1* leaf phenotype. One additional chloroplast protein is involved in chlorophyll synthesis, whereas the thylakoid rhodanese domain protein has no known function. The mitochondrial protein showing the largest increase (4.6-fold) was stomatin-like protein 1 (SLP1), localized to the inner mitochondrial membrane (Fig. 5B,C). SLP1, likely together with its homolog SLP2, forms a ~3-MDa large complex in Arabidopsis mitochondria [43]. SLP2 was also strongly increased (6.7-fold) in *fmtclpc1* relative to *clpc1* (p-value 0.013). SLP1 and SLP2 are part of the band-7/SPFH superfamily of membrane scaffold proteins [44]. Loss of SLP1 reduces protein abundance and activity of respiratory complex I, indicating a role in its assembly and/or stability [43].

We also identified four mitochondrial prohibitins (PHB1, PHB2, PHB3, and PHB6), which are members of the same superfamily [44]; however, their abundance was not increased in *fmtclpc1* compared with *clpc1*. Three additional mitochondrial proteins were increased: the membrane transporter ATM3, which exports oxidized glutathione; galactonolactone dehydrogenase (GLDH), which catalyzes the final step in ascorbate synthesis; and MTLPD1, a redox-regulated enzyme involved in photorespiration and the TCA cycle. These proteins are likely upregulated in response to mitochondrial dysfunction and stress resulting from loss of FMT. The ability of ATM3 to export GSSG has been implicated in helping to stabilize against excessive glutathione oxidation in mitochondria and thereby maintaining a suitable redox potential [59].

The 32 reduced proteins (*fmtclpc1* compared with *clpc1*) were distributed across chloroplasts (14), mitochondria (3), or other cellular compartments, encompassing diverse functions, particularly plastid fatty acid and lipid metabolism and plastid RNA-related processes (Fig. 5C). The most strongly decreased proteins included FMT (as expected), cytosolic HSP90-1 involved in protein folding, the chloroplast thylakoid protein LIL1.2/ELIP2 [60], the chloroplast pyruvate dehydrogenase E1-β subunit (PDH-Eβ) involved in acetyl-CoA synthesis for fatty acid biosynthesis, a chloroplast DEAD/DEAH-box helicase of unknown function, the essential mitochondrial intermembrane space protein TIM10 involved in protein sorting, and the chloroplast inner envelope pyruvate importer BASS2 [61]. LIL1.2/ELIP2 reduces chlorophyll levels by inhibiting chlorophyll synthesis rather than increasing chlorophyll degradation, and LIL1.2/ELIP2 does not directly affect photosystem function or the electron transport chain [60]. Its low ratio (0.19) in *fmtclpc1/clpc1* is consistent with the low chlorophyll levels observed in *clpc1*. HSP90-1 is a cytosolic member of the large HSP90 family (7 members) of protein chaperones involved in protein folding, maturation, and degradation. HSP90-1 was reduced six-fold in *fmtclpc1* compared with *clpc1* (Fig. 5B,C), indicating that cytosolic folding demand is higher in *clpc1* than in the double mutant. We identified all seven HSP90 members (HSP90-1 to -7), including chloroplast cpHSP90-5, mitochondrial HSP90-6 and ER-localized HSP90-7, as well as the four cytosolic members (HSP90-1 to -4) (Fig. 5E). All HSP90 members were lower in *fmtclpc1* than *clpc1,* indicating that suppression of *clpc1* resulted in reduced folding stress (or demands) across subcellular compartments [62].

REC1 and REC2 are required for full suppression of the *clpc1-1* phenotype by *fmt*

In both our RNA-seq-based transcriptomic and MS/MS-based proteomic analyses, REC2 mRNA and protein were induced during *fmt*-mediated suppression of *clpc1-1*. Given its close phylogenetic relationship to *FMT*, we prioritized *REC2* together with its paralogs *REC1* and *REC3* for follow-up functional analysis. RT–qPCR (Fig. 6A) confirmed the RNA-seq results and was consistent with the proteomic analysis (Fig. 5D). *REC2* was increased 2.5-fold in *fmt-3clpc1-1*, and decreased to 0.6-fold in *FMT/clpc1-1* (OE#1), both relative to *clpc1-1* (Fig. 6A). In contrast, *REC1* and *REC3* transcript levels were largely unchanged, indicating that *REC2* is the only REC family member responsive to loss of *FMT* function.

To test whether loss of *REC* paralogs can substitute for loss of *FMT*, we generated *rec1-3clpc1-1*, *rec2-1clpc1-1*, and *rec3-1clpc1-1* double mutants. The *rec3-1clpc1-1* resembled *clpc1-1*, and *rec1-*

3clpc1-1 and *rec2-1clpc1-1* were smaller and more chlorotic (Fig. 6B), demonstrating that *REC* genes cannot substitute for *FMT* in mitigating *CLPC1* deficiency.

We next tested whether *REC* genes are required for *fmt*-mediated rescue. Both *fmt-3rec1-3clpc1-1* and *fmt-3rec2-1clpc1-1* exhibited intermediate phenotypes between *fmt-3clpc1-1* and *clpc1-1*, whereas *fmt-3rec3-1clpc1-1* resembled *fmt-3clpc1-1* (Fig. 6C). Pigment analyses mirrored these patterns: total chlorophyll and carotenoids were reduced in *fmt-3rec1-3clpc1-1* and *fmt-3rec2-1clpc1-1* relative to *fmt-3clpc1-1*, while *fmt-3rec3-1clpc1-1* remained unchanged (Fig. 6D). *CLPC2* transcript abundance followed the same trend—reduced in *fmt-3rec1-3clpc1-1* and *fmt-3rec2-1clpc1-1*, unchanged in *fmt-3rec3-1clpc1-1* (Fig. 6E). Together, these results show that *REC1* and *REC2* are required for full *fmt*-mediated suppression of *clpc1-1*, whereas *REC3* is dispensable. *REC1* appears to be constitutively expressed, while *REC2* is upregulated in response to the loss of *FMT*.

DISCUSSION

Our study reveals an unexpected connection between mitochondrial dysfunction and chloroplast proteostasis, showing that loss of *FMT*–a regulator of mitochondrial morphology [26,27]—enables a compensatory response that restores chloroplast function in the absence of ClpC1. Although *fmt* mutants exhibit clustered mitochondria and impaired mitochondrial dynamics, they paradoxically display improved chloroplast performance in the *clpc1* background. These findings indicate that mitochondrial perturbation in *fmt* does not simply exacerbate cellular stress but is associated with selective transcriptional and proteomic changes—most notably induction of *CLPC2*—that enable functional compensation for loss of ClpC1. A working model consistent with our genetic, transcriptomic, and proteomic data is summarized in Fig. 6F,G.

The recurrence and strength of *fmt* alleles among independent suppressors highlight a specific role for FMT in enabling compensation for ClpC1 loss. Although additional suppressor lines were recovered in the screen, none displayed the near-complete phenotypic restoration observed in *fmt* mutants, underscoring the distinctive contribution of FMT. Loss of *FMT* does not mitigate defects in other components of the Clp protease system [15,35] or chloroplast protein import [36,37], and suppression occurs independently of GUN1-dependent retrograde signaling [21,22]. Although GUN1 is known to buffer import-associated defects [62] and to stabilize specific plastid RNAs to maintain organellar gene expression [22], these responses alone are insufficient to restore chloroplast function in *clpc1*. The ability of *fmt* to suppress *clpc1* in the absence of GUN1, together with the persistence of mitochondrial abnormalities in suppressed lines, indicates that mitochondrial perturbation supports plastid recovery through a route distinct from canonical plastid-to-nucleus signaling pathways.

A key downstream effector of this compensatory response is *CLPC2*, a ClpC1 paralog. While ClpC2 plays a minor role under normal conditions [17,38] and has been implicated in responses to organelle perturbation [7], our data extend this view by showing that mitochondrial perturbation is sufficient to drive *CLPC2* transcription to levels that restore Clp-dependent proteolysis and chloroplast biogenesis. The proportional increases in *CLPC2* expression observed in native-promoter overexpression lines indicate that the promoter is not saturated in *clpc1-1*, suggesting that *fmt* derepresses *CLPC2*. Conversely, increasing *FMT* abundance reduces *CLPC2* expression and produces phenotypes resembling the *clpc1-1clpc2-2* double mutant, consistent with an indirect, dose-dependent negative influence of *FMT* on *CLPC2* expression.

The integrated RNA-seq and comparative proteomics analyses provide critical context for this genetic compensation. Rather than revealing activation of a dominant stress or retrograde signaling pathway, these datasets show coordinated remodeling of nuclear gene expression and chloroplast protein investment in *fmtclpc1*. Transcriptome profiling indicates partial restoration of photosynthesis-associated gene expression and attenuation of plastid proteotoxic stress signatures, accompanied by selective remodeling of stress- and signaling-associated gene clusters. Notably, Cluster III highlights genes involved in hormonal (JA- and SA-related) and metabolic adjustment that are selectively enriched in *fmtclpc1*, supporting the idea that suppression involves entry into a distinct adaptive cellular state rather than engagement of a linear signaling cascade. Comparative proteomics reinforces this interpretation by demonstrating recovery of chloroplast protein accumulation and reduced cytosolic chaperone burden, consistent with improved plastid function rather than a generalized stress response. Genetic and proteomic analyses further implicate REC proteins in linking mitochondrial perturbation to *CLPC2* induction. *REC2* is strongly enriched in *fmtclpc1*, and both *REC1* and *REC2* are required for full *fmt*-mediated suppression, whereas *REC3* appears dispensable. Together with previous studies showing roles for REC proteins in plastid compartment size [31,32] and plastid-related gene expression [32], our findings support a working model in which *REC1* and *REC2* act genetically upstream of *CLPC2* induction and contribute to the broader remodeling of plastid proteostasis in the *fmt–clpc1* context.

Previous work has identified GOLDEN2-LIKE and B-BOX transcription factors as components of transcriptional networks linking chloroplast functional status with nuclear gene regulation [63]. In our study, *GLK1* and *BBX15* showed genotype-dependent expression changes across *clpc1*, *fmt*, and *fmtclpc1*, indicating responsiveness to altered chloroplast proteostasis. By contrast, GLK2, BBX14, and BBX16 did not exhibit coordinated expression changes, suggesting context-dependent engagement of the GLK–BBX regulatory network.

Together, these findings support a model in which mitochondrial perturbation exposes a latent capacity for inter-organelle compensation, enabling selective transcriptional and proteomic remodeling that restores chloroplast proteostasis when ClpC1 function is compromised.

REFERENCES

1 Sun, Y. & Jarvis, R. P. Chloroplast Proteostasis: Import, Sorting, Ubiquitination, and Proteolysis. *Annu Rev Plant Biol* **74**, 259–283 (2023). https://doi.org/10.1146/annurev-arplant-070122-032532

2 Gao, L. L., Hong, Z. H., Wang, Y. & Wu, G. Z. Chloroplast proteostasis: A story of birth, life, and death. *Plant Commun* **4**, 100424 (2023). https://doi.org/10.1016/j.xplc.2022.100424

3 Sun, J. L., Li, J. Y., Wang, M. J., Song, Z. T. & Liu, J. X. Protein Quality Control in Plant Organelles: Current Progress and Future Perspectives. *Mol Plant* **14**, 95–114 (2021). https://doi.org/10.1016/j.molp.2020.10.011

4 Woodson, J. D. & Chory, J. Coordination of gene expression between organellar and nuclear genomes. *Nat Rev Genet* **9**, 383–395 (2008). https://doi.org/10.1038/nrg2348

5 Llamas, E. & Pulido, P. A proteostasis network safeguards the chloroplast proteome. *Essays Biochem* **66**, 219–228 (2022). https://doi.org/10.1042/EBC20210058

6 van Wijk, K. J. Intra-chloroplast proteases: A holistic network view of chloroplast proteolysis. *Plant Cell* **36**, 3116–3130 (2024). https://doi.org/10.1093/plcell/koae178

7 Lopez, B. *et al.* Mutant noxy8 exposes functional specificities between the chloroplast chaperones CLPC1 and CLPC2 in the response to organelle stress and plant defence. *Plant Cell Environ* **47**, 2336–2350 (2024). https://doi.org/10.1111/pce.14882

8 Rodriguez-Concepcion, M., D'Andrea, L. & Pulido, P. Control of plastidial metabolism by the Clp protease complex. *J Exp Bot* **70**, 2049–2058 (2019). https://doi.org/10.1093/jxb/ery441

9 Bouchnak, I. & van Wijk, K. J. Structure, function, and substrates of Clp AAA+ protease systems in cyanobacteria, plastids, and apicoplasts: A comparative analysis. *J Biol Chem* **296**, 100338 (2021). https://doi.org/10.1016/j.jbc.2021.100338

10 Kim, J. *et al.* Subunits of the plastid ClpPR protease complex have differential contributions to embryogenesis, plastid biogenesis, and plant development in Arabidopsis. *Plant Cell* **21**, 1669–1692 (2009). https://doi.org/10.1105/tpc.108.063784

11 Sjogren, L. L., Stanne, T. M., Zheng, B., Sutinen, S. & Clarke, A. K. Structural and functional insights into the chloroplast ATP-dependent Clp protease in Arabidopsis. *Plant Cell* **18**, 2635–2649 (2006). https://doi.org/10.1105/tpc.106.044594

12 Olinares, P. D., Kim, J., Davis, J. I. & van Wijk, K. J. Subunit stoichiometry, evolution, and functional implications of an asymmetric plant plastid ClpP/R protease complex in Arabidopsis. *Plant Cell* **23**, 2348–2361 (2011). https://doi.org/10.1105/tpc.111.086454

13 Kim, J. *et al.* Modified Clp protease complex in the ClpP3 null mutant and consequences for chloroplast development and function in Arabidopsis. *Plant Physiol* **162**, 157–179 (2013). https://doi.org/10.1104/pp.113.215699

14 Nishimura, K. *et al.* Discovery of a Unique Clp Component, ClpF, in Chloroplasts: A Proposed Binary ClpF-ClpS1 Adaptor Complex Functions in Substrate Recognition and Delivery. *Plant Cell* **27**, 2677–2691 (2015). https://doi.org/10.1105/tpc.15.00574

15 Kim, J. *et al.* Structures, Functions, and Interactions of ClpT1 and ClpT2 in the Clp Protease System of Arabidopsis Chloroplasts. *Plant Cell* **27**, 1477–1496 (2015). https://doi.org/10.1105/tpc.15.00106

16 Sjogren, L. L. & Clarke, A. K. Assembly of the chloroplast ATP-dependent Clp protease in Arabidopsis is regulated by the ClpT accessory proteins. *Plant Cell* **23**, 322–332 (2011). https://doi.org/10.1105/tpc.110.082321

17 Nishimura, K. *et al.* ClpS1 is a conserved substrate selector for the chloroplast Clp protease system in Arabidopsis. *Plant Cell* **25**, 2276–2301 (2013). https://doi.org/10.1105/tpc.113.112557

18 Tapken, W., Kim, J., Nishimura, K., van Wijk, K. J. & Pilon, M. The Clp protease system is required for copper ion-dependent turnover of the PAA2/HMA8 copper transporter in chloroplasts. *New Phytol* **205**, 511–517 (2015). https://doi.org/10.1111/nph.13093
19 Rei Liao, J. Y. *et al.* Proteomics, phylogenetics, and coexpression analyses indicate novel interactions in the plastid CLP chaperone-protease system. *J Biol Chem* **298**, 101609 (2022). https://doi.org/10.1016/j.jbc.2022.101609
20 Paila, Y. D., Richardson, L. G. L. & Schnell, D. J. New insights into the mechanism of chloroplast protein import and its integration with protein quality control, organelle biogenesis and development. *J Mol Biol* **427**, 1038–1060 (2015). https://doi.org/10.1016/j.jmb.2014.08.016
21 Richter, A. S. *et al.* Retrograde signaling in plants: A critical review focusing on the GUN pathway and beyond. *Plant Commun* **4**, 100511 (2023). https://doi.org/10.1016/j.xplc.2022.100511
22 Tang, Q. *et al.* GENOMES UNCOUPLED PROTEIN1 binds to plastid RNAs and promotes their maturation. *Plant Commun* **5**, 101069 (2024). https://doi.org/10.1016/j.xplc.2024.101069
23 Chustecki, J. M., Etherington, R. D., Gibbs, D. J. & Johnston, I. G. Altered collective mitochondrial dynamics in the Arabidopsis msh1 mutant compromising organelle DNA maintenance. *J Exp Bot* **73**, 5428–5439 (2022). https://doi.org/10.1093/jxb/erac250
24 Nakamura, S. *et al.* Autophagy Contributes to the Quality Control of Leaf Mitochondria. *Plant Cell Physiol* **62**, 229–247 (2021). https://doi.org/10.1093/pcp/pcaa162
25 Kacprzak, S. M. & Van Aken, O. FRIENDLY is required for efficient dark-induced mitophagy and controlled senescence in Arabidopsis. *Free Radic Biol Med* **204**, 1–7 (2023). https://doi.org/10.1016/j.freeradbiomed.2023.04.007
26 El Zawily, A. M. *et al.* FRIENDLY regulates mitochondrial distribution, fusion, and quality control in Arabidopsis. *Plant Physiol* **166**, 808–828 (2014). https://doi.org/10.1104/pp.114.243824
27 Logan, D. C., Scott, I. & Tobin, A. K. The genetic control of plant mitochondrial morphology and dynamics. *Plant J* **36**, 500–509 (2003). https://doi.org/10.1046/j.1365-313x.2003.01894.x
28 Hemono, M. *et al.* FRIENDLY (FMT) is an RNA binding protein associated with cytosolic ribosomes at the mitochondrial surface. *Plant J* **112**, 309–321 (2022). https://doi.org/10.1111/tpj.15962
29 Ayabe, H. *et al.* FMT, a protein that affects mitochondrial distribution, interacts with translation-related proteins in Arabidopsis thaliana. *Plant Cell Rep* **40**, 327–337 (2021). https://doi.org/10.1007/s00299-020-02634-9
30 Ma, J. *et al.* Friendly mediates membrane depolarization-induced mitophagy in Arabidopsis. *Curr Biol* **31**, 1931–1944 e1934 (2021). https://doi.org/10.1016/j.cub.2021.02.034
31 Larkin, R. M. *et al.* REDUCED CHLOROPLAST COVERAGE genes from Arabidopsis thaliana help to establish the size of the chloroplast compartment. *Proc Natl Acad Sci U S A* **113**, E1116–1125 (2016). https://doi.org/10.1073/pnas.1515741113
32 Hu, Q. *et al.* REDUCED CHLOROPLAST COVERAGE proteins are required for plastid proliferation and carotenoid accumulation in tomato. *Plant Physiol* **196**, 511–534 (2024). https://doi.org/10.1093/plphys/kiae275
33 Gao, Y. & Zhao, Y. Epigenetic suppression of T-DNA insertion mutants in Arabidopsis. *Mol Plant* **6**, 539–545 (2013). https://doi.org/10.1093/mp/sss093
34 Jia, X., Chanda, B., Zhao, M., Brunner, A. M. & Beers, E. P. Instability of the Arabidopsis mutant csn5a-2 caused by epigenetic modification of intronic T-DNA. *Plant Sci* **238**, 53–63 (2015). https://doi.org/10.1016/j.plantsci.2015.05.015
35 Rudella, A., Friso, G., Alonso, J. M., Ecker, J. R. & van Wijk, K. J. Downregulation of ClpR2 leads to reduced accumulation of the ClpPRS protease complex and defects in chloroplast biogenesis in Arabidopsis. *Plant Cell* **18**, 1704–1721 (2006). https://doi.org/10.1105/tpc.106.042861

36 Kubis, S. *et al.* The Arabidopsis ppi1 mutant is specifically defective in the expression, chloroplast import, and accumulation of photosynthetic proteins. *Plant Cell* **15**, 1859–1871 (2003). https://doi.org/10.1105/tpc.012955
37 Bedard, J. *et al.* Suppressors of the Chloroplast Protein Import Mutant tic40 Reveal a Genetic Link between Protein Import and Thylakoid Biogenesis. *Plant Cell* **29**, 1726–1747 (2017). https://doi.org/10.1105/tpc.16.00962
38 Kovacheva, S., Bédard, J., Wardle, A., Patel, R. & Jarvis, P. Further in vivo studies on the role of the molecular chaperone, Hsp93, in plastid protein import. *Plant J.* **50**, 364–379 (2007). https://doi.org/10.1111/j.1365-313X.2007.03060.x
39 Thimm, O. *et al.* MAPMAN: a user-driven tool to display genomics data sets onto diagrams of metabolic pathways and other biological processes. *Plant J* **37**, 914–939 (2004). https://doi.org/10.1111/j.1365-313x.2004.02016.x
40 Elhafez, D. *et al.* Characterization of mitochondrial alternative NAD(P)H dehydrogenases in Arabidopsis: intraorganelle location and expression. *Plant Cell Physiol* **47**, 43–54 (2006). https://doi.org/10.1093/pcp/pci221
41 Selinski, J., Scheibe, R., Day, D. A. & Whelan, J. Alternative Oxidase Is Positive for Plant Performance. *Trends Plant Sci* **23**, 588–597 (2018). https://doi.org/10.1016/j.tplants.2018.03.012
42 Wang, Y. *et al.* Linking mitochondrial and chloroplast retrograde signalling in plants. *Philos Trans R Soc Lond B Biol Sci* **375**, 20190410 (2020). https://doi.org/10.1098/rstb.2019.0410
43 Gehl, B., Lee, C. P., Bota, P., Blatt, M. R. & Sweetlove, L. J. An Arabidopsis stomatin-like protein affects mitochondrial respiratory supercomplex organization. *Plant Physiol* **164**, 1389–1400 (2014). https://doi.org/10.1104/pp.113.230383
44 Gehl, B. & Sweetlove, L. J. Mitochondrial Band-7 family proteins: scaffolds for respiratory chain assembly? *Front Plant Sci* **5**, 141 (2014). https://doi.org/10.3389/fpls.2014.00141
45 Waters, E. R. & Vierling, E. Plant small heat shock proteins - evolutionary and functional diversity. *New Phytol* **227**, 24–37 (2020). https://doi.org/10.1111/nph.16536
46 Lama, S. *et al.* Neofunctionalization of Mitochondrial Proteins and Incorporation into Signaling Networks in Plants. *Mol Biol Evol* **36**, 974–989 (2019). https://doi.org/10.1093/molbev/msz031
47 Bittner, A. *et al.* Organelles and phytohormones: a network of interactions in plant stress responses. *J Exp Bot* **73**, 7165–7181 (2022). https://doi.org/10.1093/jxb/erac384
48 Rekhter, D. *et al.* Isochorismate-derived biosynthesis of the plant stress hormone salicylic acid. *Science* **365**, 498–502 (2019). https://doi.org/10.1126/science.aaw1720
49 Brownfield, D. L., Todd, C. D. & Deyholos, M. K. Analysis of Arabidopsis arginase gene transcription patterns indicates specific biological functions for recently diverged paralogs. *Plant Mol Biol* **67**, 429–440 (2008). https://doi.org/10.1007/s11103-008-9336-2
50 Morikawa, K., Shiina, T., Murakami, S. & Toyoshima, Y. Novel nuclear-encoded proteins interacting with a plastid sigma factor, Sig1, in Arabidopsis thaliana. *FEBS Lett* **514**, 300–304 (2002). https://doi.org/10.1016/s0014-5793(02)02388-8
51 Xie, Y. D. *et al.* The Arabidopsis gene SIGMA FACTOR-BINDING PROTEIN 1 plays a role in the salicylate- and jasmonate-mediated defence responses. *Plant Cell Environ* **33**, 828–839 (2010). https://doi.org/10.1111/j.1365-3040.2009.02109.x
52 Zhang, H. *et al.* Arabidopsis SIGMA FACTOR BINDING PROTEIN1 (SIB1) and SIB2 inhibit WRKY75 function in abscisic acid-mediated leaf senescence and seed germination. *J Exp Bot* **73**, 182–196 (2022). https://doi.org/10.1093/jxb/erab391
53 Wang, Y. *et al.* Stress responsive mitochondrial proteins in Arabidopsis thaliana. *Free Radic Biol Med* **122**, 28–39 (2018). https://doi.org/10.1016/j.freeradbiomed.2018.03.031
54 He, C. *et al.* Co-regulation of mitochondrial and chloroplast function: Molecular components and mechanisms. *Plant Commun* **4**, 100496 (2023). https://doi.org/10.1016/j.xplc.2022.100496

55 Hernandez-Verdeja, T. Regulation of Chloroplast Biogenesis and Differentiation. *J Exp Bot* (2025). https://doi.org/10.1093/jxb/eraf530

56 Ohmiya, A., Oda-Yamamizo, C. & Kishimoto, S. Overexpression of CONSTANS-like 16 enhances chlorophyll accumulation in petunia corollas. *Plant Sci* **280**, 90–96 (2019). https://doi.org/10.1016/j.plantsci.2018.11.013

57 Lee, K. P. *et al.* Hierarchical regulatory module GENOMES UNCOUPLED1-GOLDEN2-LIKE1/2-WRKY18/40 modulates salicylic acid signaling. *Plant Physiol* **192**, 3120–3133 (2023). https://doi.org/10.1093/plphys/kiad251

58 Atanasov, V. *et al.* Arabidopsis BBX14 is involved in high light acclimation and seedling development. *Plant J* **118**, 141–158 (2024). https://doi.org/10.1111/tpj.16597

59 Marty, L. *et al.* Arabidopsis glutathione reductase 2 is indispensable in plastids, while mitochondrial glutathione is safeguarded by additional reduction and transport systems. *New Phytol* **224**, 1569–1584 (2019). https://doi.org/10.1111/nph.16086

60 Tzvetkova-Chevolleau, T. *et al.* The light stress-induced protein ELIP2 is a regulator of chlorophyll synthesis in Arabidopsis thaliana. *Plant J* **50**, 795–809 (2007). https://doi.org/10.1111/j.1365-313X.2007.03090.x

61 Furumoto, T. *et al.* A plastidial sodium-dependent pyruvate transporter. *Nature* **476**, 472–475 (2011). https://doi.org/10.1038/nature10250

62 Wu, G. Z. *et al.* Control of retrograde signalling by protein import and cytosolic folding stress. *Nat Plants* **5**, 525–538 (2019). https://doi.org/10.1038/s41477-019-0415-y

63 Susila, H. *et al.* Chloroplasts prevent precocious flowering through a GOLDEN2-LIKE-B-BOX DOMAIN PROTEIN module. *Plant Commun* **4**, 100515 (2023). https://doi.org/10.1016/j.xplc.2023.100515

64 Kim, Y., Schumaker, K. S. & Zhu, J. K. EMS mutagenesis of Arabidopsis. *Methods Mol Biol* **323**, 101–103 (2006). https://doi.org/10.1385/1-59745-003-0:101

65 Wachsman, G., Modliszewski, J. L., Valdes, M. & Benfey, P. N. A SIMPLE Pipeline for Mapping Point Mutations. *Plant Physiol* **174**, 1307–1313 (2017). https://doi.org/10.1104/pp.17.00415

66 Bae, N. *et al.* Enhanced salt stress tolerance in plants without growth penalty through increased photosynthesis activity by plastocyanin from Antarctic moss. *Plant J* **121**, e17168 (2025). https://doi.org/10.1111/tpj.17168

67 Chen, Y. *et al.* SOAPnuke: a MapReduce acceleration-supported software for integrated quality control and preprocessing of high-throughput sequencing data. *Gigascience* **7**, 1–6 (2018). https://doi.org/10.1093/gigascience/gix120

68 Liao, Y., Smyth, G. K. & Shi, W. featureCounts: an efficient general purpose program for assigning sequence reads to genomic features. *Bioinformatics* **30**, 923–930 (2014). https://doi.org/10.1093/bioinformatics/btt656

69 Love, M. I., Huber, W. & Anders, S. Moderated estimation of fold change and dispersion for RNA-seq data with DESeq2. *Genome Biol* **15**, 550 (2014). https://doi.org/10.1186/s13059-014-0550-8

70 Friso, G., Olinares, P. D. & van Wijk, K. J. The workflow for quantitative proteome analysis of chloroplast development and differentiation, chloroplast mutants, and protein interactions by spectral counting. *Methods Mol Biol* **775**, 265–282 (2011). https://doi.org/10.1007/978-1-61779-237-3_14

Acknowledgments

This research was supported by the following grants: National Research Foundation of Korea (2019R1I1A1A01064009 and RS-2023-00247582 to J.K., RS-2023-00208784 to D.W.L., RS-2024-00407469 and RS-2025-00564152 to B.h.L., and NRF-2022R1A3B1078180 to J.H.A.), and a US National Science Foundation grant MCB-2322813 to K.J.v.W.

Author contributions:

J.K. conceived the experiments, and K.J.v.W. conceived the multi-omics experiments. J.K. performed EMS screening, all genetic crosses, and data analysis. K.J.v.W. and P.R. performed quantitative comparative proteomics and RNA-seq analyses, while Z.N. conducted the initial RNA-seq analysis. N.S. and H.L. provided bioinformatics consultation and support. J.K., C.N., and D.B.K. performed biochemical experiments, including total and chloroplast protein extraction and immunoblotting. J.K., D.B.K., and J.-Y.K. performed cloning. C.N. carried out the PAA2 degradation assay, and J.-Y.K. generated CRISPR/Cas9 lines. J.K., N.B., and H.K. performed RT-PCR analyses. J.K. prepared samples for RNA-seq and proteomics. J.K., C.N., N.B., H.K., D.B.K., R.L., J.H.K., and G.C. performed plant transformation and/or other molecular genetic experiments. J.K., J.H.A., B.h.L., D.W.L., and K.J.v.W. supervised the project and analyzed and interpreted the data. J.K. and K.J.v.W. wrote the manuscript. D.W.L. and P.R. reviewed, edited, and provided substantive feedback on the manuscript. C.N., N.B., H.K., J.-Y.K., D.B.K., N.S., Z.N., R.L., J.H.K., G.C., H.L., and B.h.L. reviewed the manuscript and provided additional comments and/or editorial suggestions.

Competing interests: Authors declare that they have no competing interests.

Data and materials availability

MS-based protein identifications are available through the Plant Proteome Data Base (PPDB) under experiment ids #2599-2604. MS-based protein quantifications are available in the Supplementary Data Sets.

Supplementary Materials

Supplementary Figures 1-5

Supplementary Tables 1-3

Supplementary Data Sets 1 and 2

FIGURE LEGENDS

Figure 1. Identification and confirmation of *FMT* as the causal gene for suppressor mutations of *clpc1-1*.

(A) Workflow of EMS mutagenesis, suppressor screening, and bulked segregant analysis. Seeds of *clpc1-1* were mutagenized with ethyl methanesulfonate (EMS) (~10,000 seeds), and M2 plants were screened for suppressor mutants exhibiting a green-leaf phenotype. Selected M2 plants were backcrossed to the parental *clpc1-1* line (M0) to generate BC1F2 progeny. Pooled DNA from green BC1F2 plants was subjected to whole-genome sequencing (WGS), and mutations were identified using the SIMPLE pipeline (Wachsman et al., 2017).

(B) Growth and development of wild-type (Col-0), *clpc1-1*, and four independent *clpc1-1* suppressor mutants - designated *socc* (suppressor of *clpc1*) - including *socc20-1 clpc1-1*, *socc20-4 clpc1-1*, *socc39-1 clpc1-1*, and *socc43-1 clpc1-1*, grown on soil for 23 days under a 16/8 hour light/dark cycle at 100 µmol photons m^{-2} s^{-1}. Scale bar = 2 cm.

(C) Gene model of *FMT* (At3g52140) showing the positions of T-DNA insertions (*fmt-3*, *fmt-4*) and EMS-induced mutations identified in *socc* suppressor lines. Coding exons (black boxes), untranslated regions (open boxes), and introns (gray lines) are indicated. Mutation sites are mapped relative to the *FMT* genomic structure. The EMS-induced *socc* alleles include canonical splice-site defects and splice-region variants that disrupt *FMT* coding or splicing, while the T-DNA alleles (*fmt-3* and *fmt-4*) interrupt the gene's exon–intron structure. These mutations affect *FMT* coding or splicing and are associated with the corresponding mutant phenotypes. Detailed mutation positions, nucleotide changes, and predicted effects are provided in table S1.

(D) Genetic complementation of four suppressor mutants (*socc clpc1-1* lines) using a genomic *FMT* transgene driven by its native promoter. Transformation of each *socc clpc1-1* mutant with *pFMT:FMT* restored the yellow, chlorotic phenotype characteristic of *clpc1-1*, confirming *FMT* as the causal gene. Plants were grown on soil for 18 days under a 16/8 hour light/dark cycle at 100 µmol photons m^{-2} s^{-1}. Scale bar = 2 cm.

(E) T-DNA insertion alleles *fmt-3* and *fmt-4* suppress the *clpc1-1* phenotype, similar to EMS-derived suppressor lines. Growth and development of wild-type, *fmt-3*, *fmt-4*, *clpc1-1*, *fmt-3 clpc1-1*, and *fmt-4 clpc1-1* plants grown on soil for 23 days under a 16/8 hour light/dark cycle at 100 µmol photons m^{-2} s^{-1}. Scale bar = 2 cm.

(F) Photosynthetic efficiency and pigment accumulation in wild type, *fmt-3, clpc1-1*, and suppressor lines. Maximum quantum efficiency of PSII (Fv/Fm), total chlorophyll content, and total carotenoid content were measured in Col-0 (wild type), *fmt-3*, *clpc1-1*, *fmt-3 clpc1-1*, and *socc20-1 clpc1-1*. Fv/Fm measurements were performed on 22–24-day-old soil-grown plants,

while pigment quantifications were conducted on 21-day-old plants, all grown under a 16/8 hour light/dark cycle at 100 µmol photons m^{-2} s^{-1}. Fv/Fm values (left), total chlorophyll (middle), and total carotenoid contents (right) are shown. Chlorophyll and carotenoid contents are expressed as micrograms per milligram fresh weight (µg/mg FW). Bars represent mean ± SD (n = 7 for Fv/Fm; n = 5 for chlorophyll and carotenoid contents). Different lowercase letters indicate groups that differ significantly, as determined by one-way ANOVA followed by Tukey's range test ($P < 0.05$).

(G) Suppression of CRISPR/Cas9-derived *clpc1* mutant alleles (*clpc1-4* and *clpc1-5*) by *fmt-3*. Growth and development of wild-type, *clpc1-1*, *clpc1-4*, *clpc1-5*, *fmt-3*, *fmt-3 clpc1-1*, *fmt-3 clpc1-4*, and *fmt-3 clpc1-5* plants grown on soil for 20 days under a 16/8 hour light/dark cycle at 100 µmol photons m^{-2} s^{-1}. Scale bar = 2 cm.

Figure 2. Genetic Interaction of various mutants with *fmt*.

(A) Growth and development of *clpr2-1, fmt-3 clpr2-1,* and *fmt-4 clpr2-1* mutants. Plants were grown on soil for 22 days under a 16/8 hour light/dark cycle at 100 µmol photons m^{-2} s^{-1}. Scale bar = 1 cm.

(B) Growth and development of *clpt1-2 clpt2-1* and *fmt-4 clpt1-2 clpt2-1* mutants. Plants were grown on soil for 29 days under the same conditions. Scale bar = 1 cm.

(C) Growth and development of *fmt-3, ppi1-1,* and *fmt-3 ppi1-1* mutants. Plants were grown on soil for 24 days under the same conditions. Scale bar = 2 cm.

(D) Growth and development of *fmt-3, fmt-4, tic40-4, fmt-3 tic40-4,* and *fmt-4 tic40-4* mutants. Plants were grown on soil for 20 days under the same conditions. Scale bar = 2 cm.

(E) Growth and development of wild-type (Col-0), *fmt-3*, *fmt-4*, *socc20-1*, *gun1-101*, *fmt-3 gun1-101*, *fmt-4 gun1-101*, and *socc20-1 gun1-101* plants grown on soil for 21 days under a 16/8 hour light/dark cycle at 100 µmol photons m^{-2} s^{-1}. Variegated phenotypes were observed in all *fmt gun1-101* double mutants. Scale bar = 2 cm.

(F) Growth and development of *clpc1-1*, *fmt-3 clpc1-1*, *fmt-4 clpc1-1*, *socc20-1 clpc1-1*, *clpc1-1 gun1-101*, *fmt-3 clpc1-1 gun1-101*, *fmt-4 clpc1-1 gun1-101*, and *socc20-1 clpc1-1 gun1-101* plants grown on soil for 21 days under a 16/8 hour light/dark cycle at 100 µmol photons m^{-2} s^{-1}. Suppression of the *clpc1-1 gun1-101* growth defect was observed in all *fmt clpc1-1 gun1-101* triple mutants. Scale bar = 2 cm.

Figure 3. Loss of FMT restores chloroplast morphology and protease activity through compensatory upregulation of *CLPC2*.

(A) Chloroplast ultrastructure in *fmt-3clpc1-1* and *clpc1-1*. Left panel: Transmission electron microscopy (TEM) of chloroplasts from *fmt-3 clpc1-1* leaf mesophyll cells. Chloroplasts exhibit compact morphology, well-organized grana stacks, and dense stromal regions, closely resembling wild type. Notably, mitochondria remain tightly clustered, consistent with the known *fmt* phenotype. Scale bar = 1 µm.

Right panel: TEM of chloroplasts from *clpc1-1*. Chloroplasts appear swollen and rounded, with fewer and less organized thylakoid membranes and smaller, loosely stacked grana. Stromal regions are less compact than in the double mutant. Scale bar = 1 µm. m, mitochondria; c, chloroplast.

(B) Immunoblot analysis of selected chloroplast proteins in Col-0, *clpc1-1*, *fmt-4*, *fmt-4 clpc1-1*, and *socc20-1 clpc1-1*. Antibodies used: ClpF (a Clp N-recognin adaptor protein), ClpS1 (a substrate selector for the Clp complex), and PAA2 (a Clp substrate involved in thylakoid copper transport). Each lane was loaded with either 10 µg (1×) or 30 µg (3×) of total chloroplast protein. Coomassie Brilliant Blue (CBB) staining shows equal loading.

(C) PAA2 degradation assay using total protein extracts treated with or without $CuSO_4$. In Col-0, Cu^{2+} exposure leads to decreased PAA2 levels, whereas in *clpc1-1*, PAA2 remains elevated regardless of treatment. Cu^{2+}-dependent degradation is restored in *fmt-3 clpc1-1*, *fmt-4 clpc1-1*, and *socc20-1 clpc1-1*. No degradation is observed in *fmt-3 clpr2-1*. Ponceau S staining confirms equal loading.

(D) Quantitative RT-PCR analysis of *CLPC2* transcript levels in wild type (Col-0), *fmt-3, fmt-4*, *fmt-3 clpc1-1, fmt-4 clpc1-1*, *socc20-1 clpc1-1*, *clpc1-1*, *FMT/clpc1-1* overexpression (OE) lines (#1–2), and *clpc1-1 clpc2-2*. For comparison, *CLPD* transcript levels are shown for wild type (Col-0), *fmt-3*, *fmt-3 clpc1-1*, *clpc1-1*, and *FMT/clpc1-1* OE#1. Data represent means ± SD from three biological replicates.

(E) Growth phenotype of *clpc1-1* and independent *pCLPC2:gCLPC2/clpc1-1* overexpression (OE) lines (#1–3) grown on soil for 18 days under a 16/8 hour light/dark cycle at 90 µmol photons m^{-2} s^{-1}. Scale bar = 2 cm.
(F) Total chlorophyll (a + b) accumulation in the lines shown in (E). Chlorophyll contents were quantified in 25-day-old plants grown under the same conditions and are expressed as micrograms per milligram fresh weight (µg/mg FW). Values represent mean ± SD (n = 5).
(G) RT–qPCR analysis of *CLPC1* and *CLPC2* transcript levels in the same lines shown in (E).

OE lines with higher *CLPC2* expression (e.g., OE #2 and OE #3) exhibit a greener phenotype compared with OE #1. Bars represent mean ± SD (n = 3).

(H) Growth and development of *clpc1-1*, *clpc1-1 clpc2-2*, and *FMT/clpc1-1* plants grown on soil for 17 days under a 16/8 hour light/dark cycle at 100 µmol photons m^{-2} s^{-1}. Both *clpc1-1 clpc2-2* and *FMT/clpc1-1* plants exhibited severely stunted and chlorotic phenotypes compared to *clpc1-1*. Overexpression lines were slightly larger than *clpc1-1 clpc2-2*.

(I) Photosynthetic efficiency and total chlorophyll (a + b) accumulation in the same lines shown in (H). Maximum quantum efficiency of PSII (Fv/Fm; upper) and total chlorophyll contents (lower) were measured in 24-day-old soil-grown plants grown under a 16/8 hour light/dark cycle at 100 µmol photons m^{-2} s^{-1}. Chlorophyll contents are expressed as micrograms per milligram fresh weight (µg/mg FW). Bars represent mean ± SD (n = 15 for Fv/Fm; n = 5 for chlorophyll contents). (D), (F), (G) and (I) Different lowercase letters indicate groups that differ significantly, as determined by one-way ANOVA followed by Tukey's range test ($P < 0.05$).

Figure 4. RNA expression patterns across the five genotypes wild type (Col-0), *fmt, clpc1, fmtclpc1* and *FMT/clpc1*.

(A) Principal Component Analysis (PCA) of RNA-seq data showing clustering of biological replicates by genotype.

(B) Hierarchical cluster analysis of z-score-normalized average RNA abundance of 4745 protein-coding nuclear genes in WT*, fmt, clpc1, fmtclpc1* and *FMT/clpc1* sampled at stage 1.07. Only genes that show at least one pairwise significance difference (adj $P<0.01$ and at least 2-fold difference) between 2 genotypes are included. The cladogram has three main clusters (I, II, III) with three subclusters each. The scaling of heat map is shown in the top right. The z-score was calculated as (individual value-average)/standard deviation for each gene across the 5 genotypes.

(C) MapMan functional bin distribution across clusters I, II and III for all genes in the cladogram (4745 genes). Only bins with more than 10 genes are shown.

(D) MapMan functional bin distribution of plastid and mitochondrial proteins across clusters I, II and III (638 genes). Only bins with more than 10 genes are shown.

(E) Differential expression of the transcription factors **HSFA2, GLK1, BBX15, and WRKY40**. RNA-seq–normalized counts are shown as means ± SD for each genotype. Statistical significance was assessed using ordinary one-way ANOVA with Tukey's multiple-comparison

test. Significant differences are indicated by asterisks (*$P < 0.05$, **$P < 0.01$, ***$P < 0.001$, ****$P < 0.0001$). Gene cluster membership is indicated.

Figure 5. Comparative analysis of total rosette proteomes of *clpc1* and *fmtclpc1* soil- grown seedlings in growth stage 1.07 based on NadjSPC.

(A) Bar diagram displaying the relative abundance of the chloroplast ClpPRT complex and ClpC2 in *fmtclpc1* and *clpc1*.

(B) Volcano plot of the *fmtclpc1/clpc1* relative protein abundance ratio and significance of differential accumulation. Horizontal dashed lines indicate the -log10 p-value at 0.01 and the vertical dashed lines indicate 2-fold protein abundance difference between *fmtclpc1* and *clpc1*.

(C) Differentially accumulating proteins (P<0.01; <0.5 or >2) based on NadjSPC in *clpc1* vs *fmtclpc1.*

(D) Bar diagram displaying the relative abundance of FMT and the related REC1,2,3 proteins in *fmtclpc1* and *clpc1*. *P<0.05; **P<0.01.

(E) Bar diagram displaying the relative abundance of each of the seven HSP90 proteins in *fmtclpc1* and *clpc1*. *P<0.05; **P<0.01. HSP90-1,2,3,4 are localized to the cytosol. HSP90-5,6 and 7 are respectively localized to the chloroplast (p), mitochondria (m) and endoplasmic reticulum (ER).

Figure 6. *REC1* and *REC2* are required for full suppression of *clpc1-1* by *fmt.*

(A) Quantitative RT-PCR analysis of *REC1*, *REC2*, and *REC3* transcript levels in wild type (Col-0), *fmt-3*, *fmt-3 clpc1-1*, *clpc1-1*, and *FMT/clpc1-1* OE#1. Data represent mean ± SD from three biological replicates.

(B) Growth and development of wild type, *clpc1-1*, *rec1-3*, *rec2-1*, *rec3-1*, *rec1-3 clpc1-1*, *rec2-1 clpc1-1*, and *rec3-1 clpc1-1* mutants. Plants were grown on soil for 17 days under a 16/8 hour light/dark cycle at 100 µmol photons m^{-2} s^{-1}. Scale bar = 2 cm.

(C) Growth and development of *fmt-3 rec1-3 clpc1-1*, *fmt-3 rec2-1 clpc1-1*, *fmt-3 rec3-1 clpc1-1*, *fmt-3 clpc1-1*, and *clpc1-1* mutants. Plants were grown on soil for 18 days under a 16/8 hour light/dark cycle at 100 µmol photons m^{-2} s^{-1}. Scale bar = 2 cm.

(D) Pigment accumulation in the same lines shown in (C). Total chlorophyll and carotenoid contents were measured in 21-day-old plants grown under a 16/8 hour light/dark cycle at 100 µmol photons m^{-2} s^{-1}. Total chlorophyll (left) and total carotenoids (right) are shown. Pigment contents are expressed as micrograms per milligram fresh weight (µg/mg FW). Values represent mean ± SD (n = 5).
(E) Quantitative RT-PCR analysis of *CLPC2* transcript levels were measured in *clpc1-1*, *fmt-3 clpc1-1*, *fmt-3 rec1-3 clpc1-1*, *fmt-3 rec2-1 clpc1-1*, and *fmt-3 rec3-1 clpc1-1*. Data represent mean ± SD from three biological replicates. (A), (D), and (E) Different lowercase letters indicate groups that differ significantly, as determined by one-way ANOVA followed by Tukey's range test ($P < 0.05$).

(F) *clpc1*-associated retrograde signaling state. Working model illustrating the transcriptional and physiological state of *clpc1* relative to wild type. Loss of ClpC1 causes chloroplast dysfunction, triggering plastid-to-nucleus retrograde signaling associated with a broadly repressive nuclear response. This state correlates with reduced expression of multiple transcription factors, including GLK1, and BBX15, as well as decreased expression of photosynthesis-related genes. In parallel, plastid-localized metabolic response genes such as ACC2 are upregulated, reflecting altered plastid metabolic states associated with impaired chloroplast proteostasis and the small, virescent *clpc1* phenotype. Dashed arrows denote inferred signaling relationships based on transcriptomic and phenotypic analyses.

(G) FMT-mediated recovery state in *fmtclpc1*. Working Model illustrating the transcriptional and physiological changes associated with FMT-dependent suppression of *clpc1*. Loss of *FMT*, a mitochondria-localized member of the FMT–REC gene family, is associated with mitochondrial stress signaling that engages a mitochondria-to-nucleus communication route. This nuclear response correlates with increased expression of *REC2* and *CLPC2*, the latter encoding a plastid protease chaperone that compensates for loss of ClpC1 and promotes recovery of chloroplast proteostasis in *fmtclpc1*. In this recovery state, transcription factors (TFs) associated with chloroplast gene programs (GLK1, BBX15) are upregulated. Upregulation of mitochondrial redox- and metabolism-associated factors (e.g., SLP1, SLP2, ATM3, GLDH, LPD1) is consistent with the involvement of mitochondria-derived signaling. In parallel, increased expression of salicylic acid (SA)- and jasmonic acid (JA)-related signaling components is observed, consistent with a broader stress-responsive nuclear transcriptional state. Reduced ACC2 and ELIP2 abundance, together with increased expression of photosynthesis-related genes, correlates with recovery of chloroplast function and proteostasis in *fmtclpc1*. The *fmt–clpc1* interaction occurs independently of GUN1, which is shown separately. Genes shown in red are upregulated and those in blue are downregulated based on integrated transcriptomic and proteomic datasets; dashed arrows denote inferred signaling or transcriptional relationships supported by genetic, transcriptomic, and proteomic evidence.

Fig. 1A-G

A

clpc1-1
↓
EMS mutagenesis (~10,000 M1 seeds)
↓
M2: Screen for suppressor mutants (green leaves)
↓
Cross: Selected M2 x *clpc1-1*
↓
BC1F2 segregating population
↓
Genomic DNA extraction from pooled BC1F2 → WGS
↓
SIMPLE Pipeline
↓
Candidate gene identification → Validation

B

C

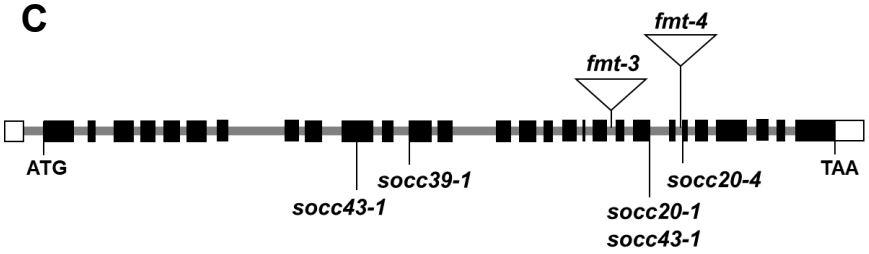

D

E

F

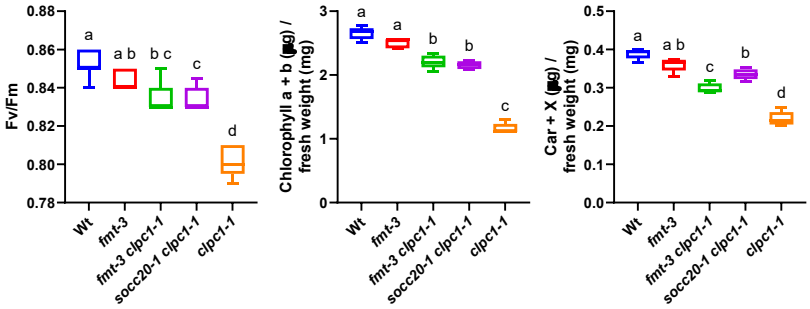

G

Fig. 2A-F

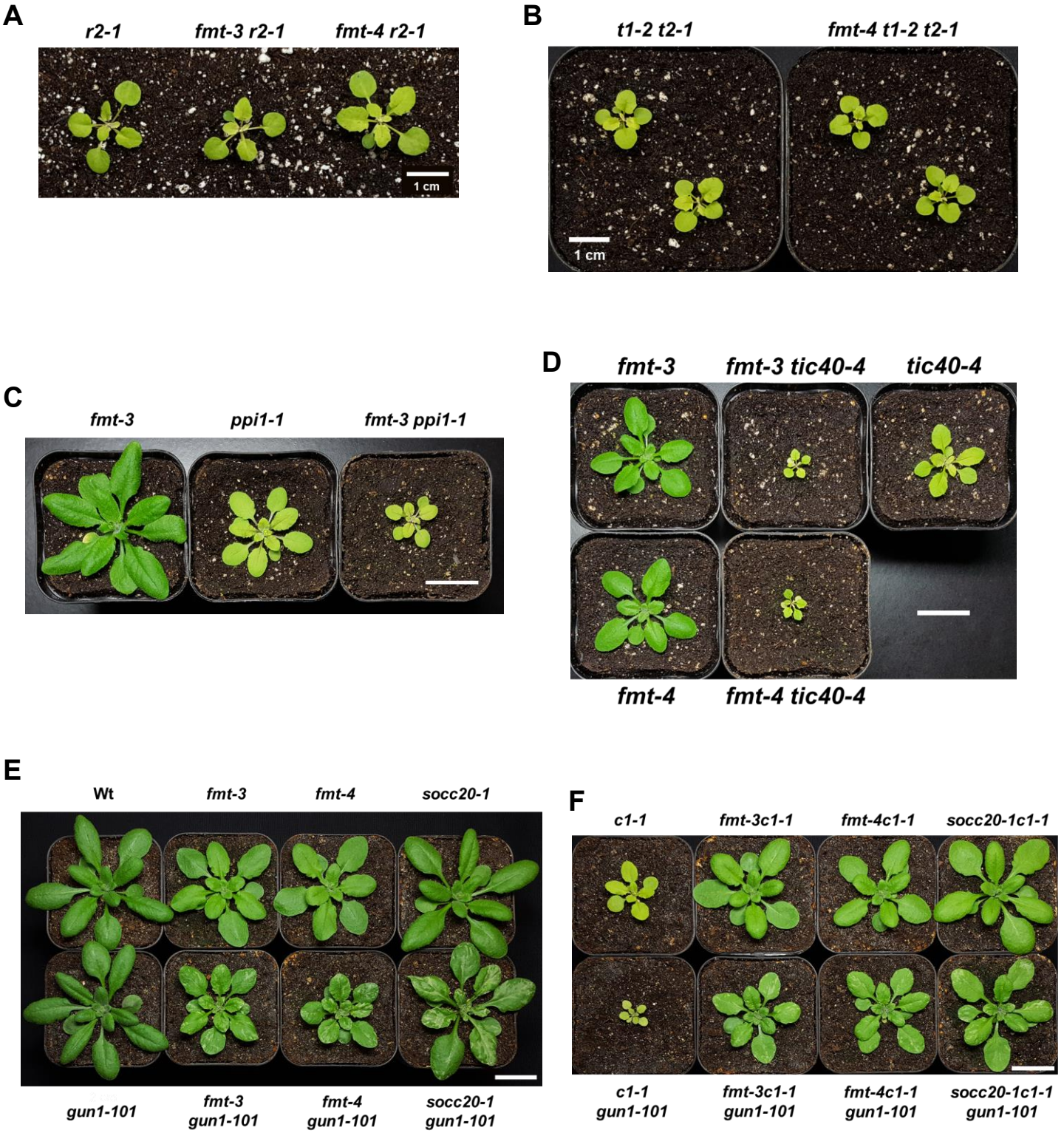
A
r2-1
fmt-3 r2-1
fmt-4 r2-1
1 cm
B
t1-2 t2-1
fmt-4 t1-2 t2-1
1 cm
C
fmt-3
ppi1-1
fmt-3 ppi1-1
D
fmt-3
fmt-3 tic40-4
tic40-4
fmt-4
fmt-4 tic40-4
E
Wt
fmt-3
fmt-4
socc20-1
gun1-101
fmt-3 gun1-101
fmt-4 gun1-101
socc20-1 gun1-101
F
c1-1
fmt-3c1-1
fmt-4c1-1
socc20-1c1-1
c1-1 gun1-101
fmt-3c1-1 gun1-101
fmt-4c1-1 gun1-101
socc20-1c1-1 gun1-101

Fig. 3A-D

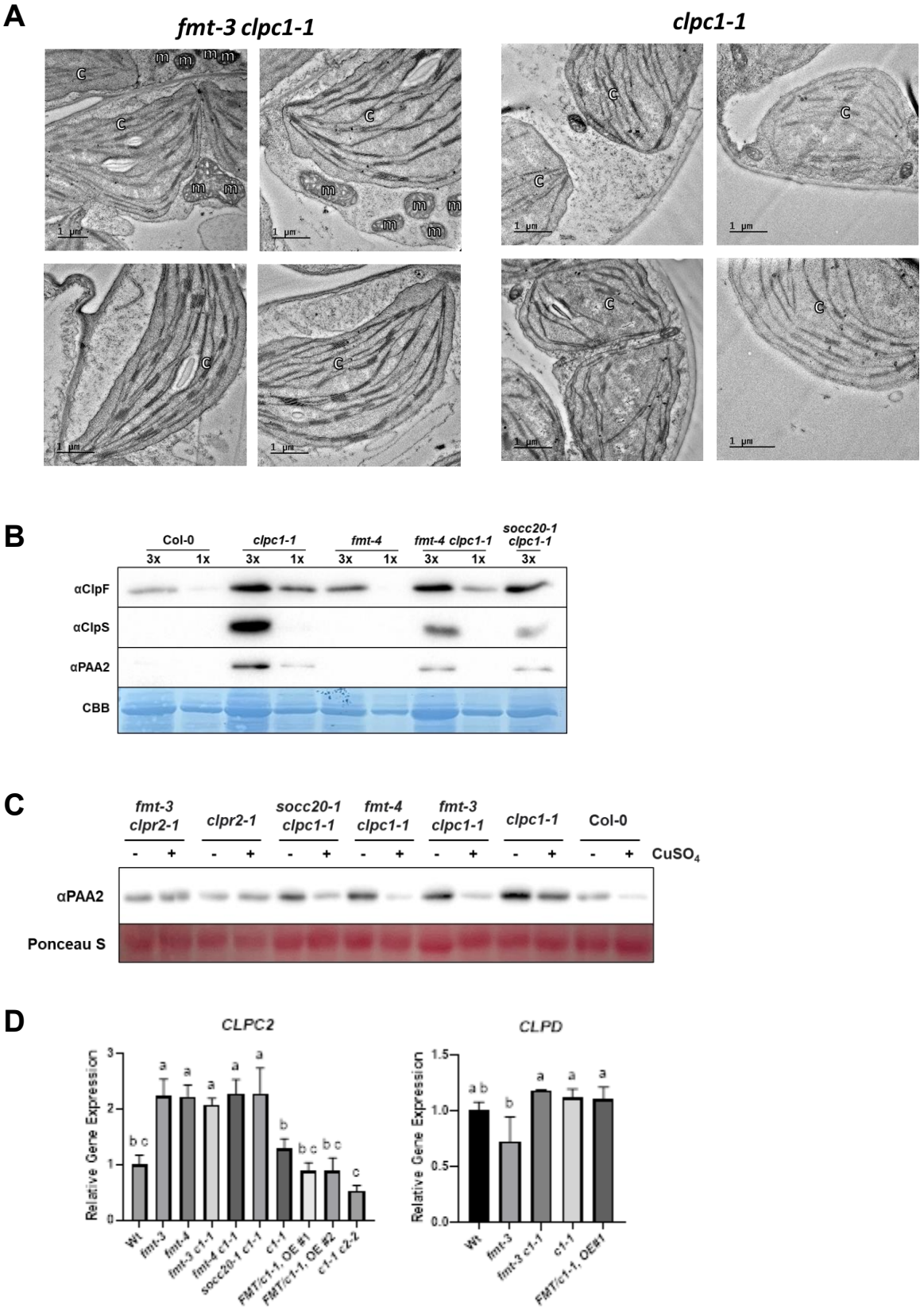
A
fmt-3 clpc1-1
clpc1-1
C
m
1 µm
B
Col-0
clpc1-1
fmt-4
fmt-4 clpc1-1
socc20-1 clpc1-1
3x
1x
αClpF
αClpS
αPAA2
CBB
C
fmt-3 clpr2-1
clpr2-1
socc20-1 clpc1-1
fmt-4 clpc1-1
fmt-3 clpc1-1
clpc1-1
Col-0
CuSO4
αPAA2
Ponceau S
D
CLPC2
CLPD
Relative Gene Expression
Wt
fmt-3
fmt-4
fmt-3 c1-1
fmt-4 c1-1
socc20-1 c1-1
c1-1
FMT/c1-1, OE #1
FMT/c1-1, OE #2
c1-1 c2-2
FMT/c1-1, OE#1

Fig. 3E-I

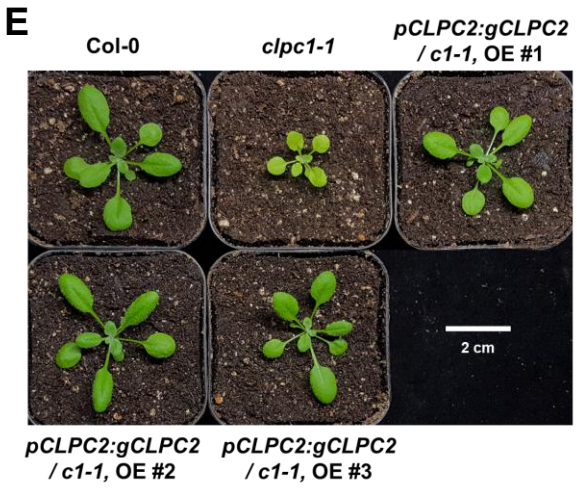
E
Col-0
clpc1-1
pCLPC2:gCLPC2 / c1-1, OE #1
2 cm
pCLPC2:gCLPC2 / c1-1, OE #2
pCLPC2:gCLPC2 / c1-1, OE #3

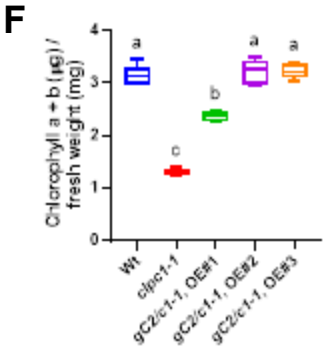
F
Chlorophyll a + b (μg) / fresh weight (mg)
Wt
clpc1-1
gC2/c1-1, OE#1
gC2/c1-1, OE#2
gC2/c1-1, OE#3

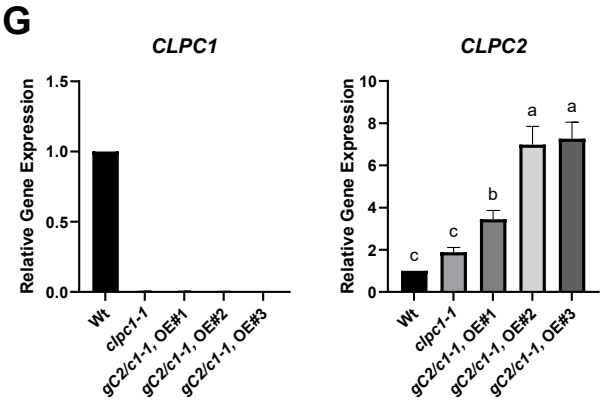
G
CLPC1
CLPC2
Relative Gene Expression
Wt
clpc1-1
gC2/c1-1, OE#1
gC2/c1-1, OE#2
gC2/c1-1, OE#3

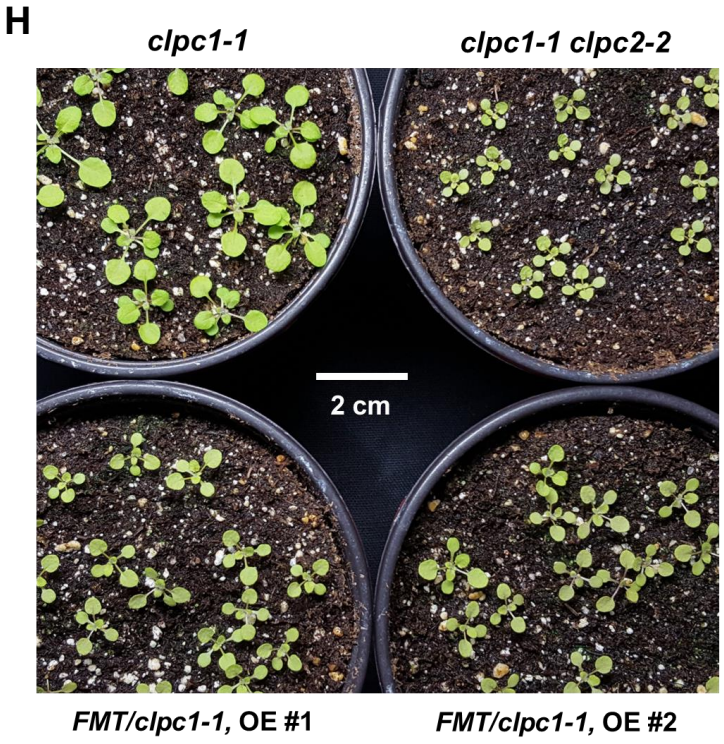
H
clpc1-1
clpc1-1 clpc2-2
2 cm
FMT/clpc1-1, OE #1
FMT/clpc1-1, OE #2

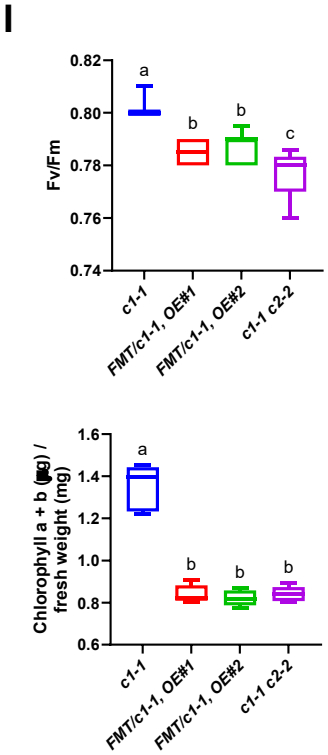
I
Fv/Fm
Chlorophyll a + b (μg) / fresh weight (mg)
c1-1
FMT/c1-1, OE#1
FMT/c1-1, OE#2
c1-1 c2-2

Fig. 4A-E

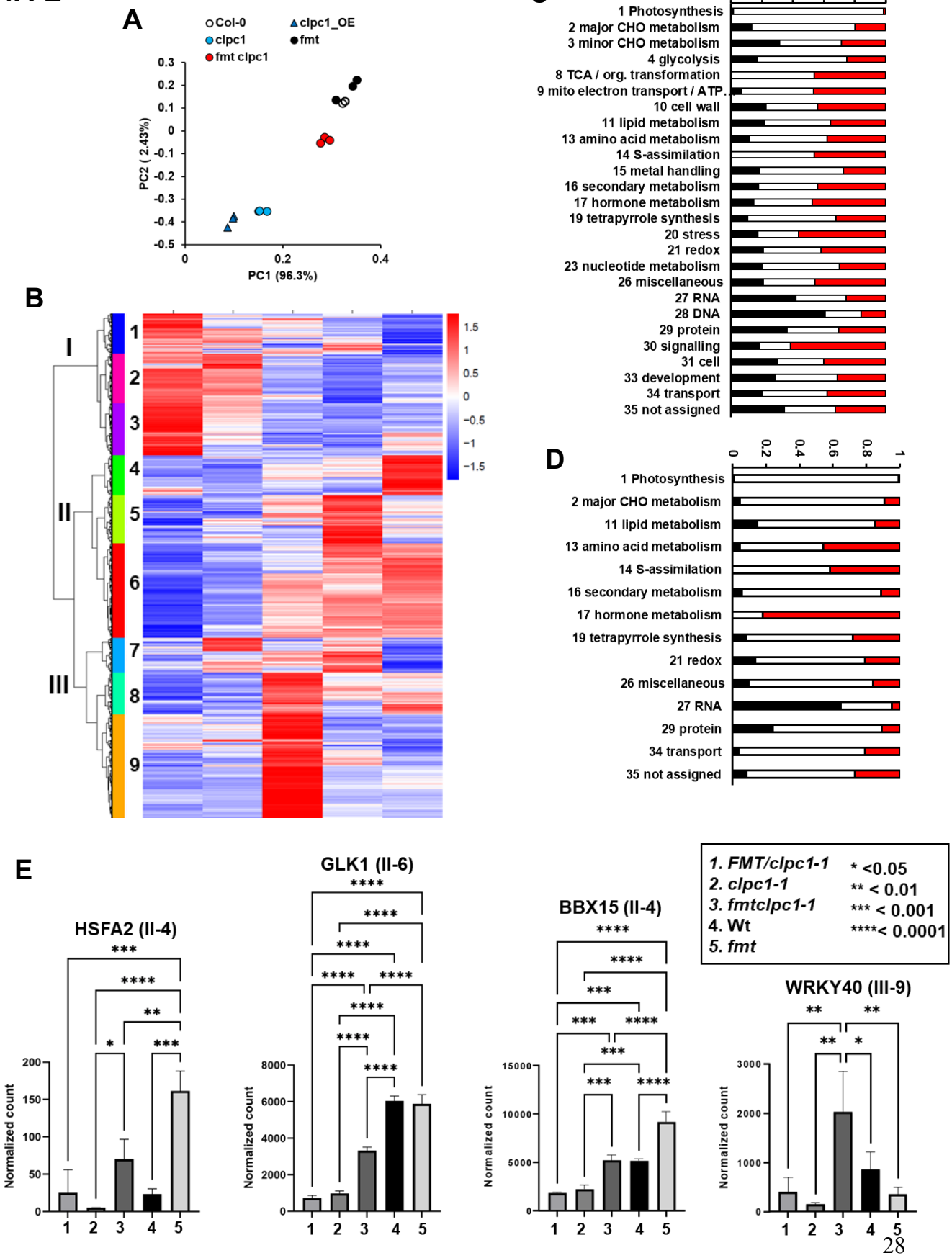
A
Col-0
clpc1
fmt clpc1
clpc1_OE
fmt
PC2 (2.43%)
PC1 (96.3%)
B
I
II
III
1
2
3
4
5
6
7
8
9
C
1 Photosynthesis
2 major CHO metabolism
3 minor CHO metabolism
4 glycolysis
8 TCA / org. transformation
9 mito electron transport / ATP..
10 cell wall
11 lipid metabolism
13 amino acid metabolism
14 S-assimilation
15 metal handling
16 secondary metabolism
17 hormone metabolism
19 tetrapyrrole synthesis
20 stress
21 redox
23 nucleotide metabolism
26 miscellaneous
27 RNA
28 DNA
29 protein
30 signalling
31 cell
33 development
34 transport
35 not assigned
D
1 Photosynthesis
2 major CHO metabolism
11 lipid metabolism
13 amino acid metabolism
14 S-assimilation
16 secondary metabolism
17 hormone metabolism
19 tetrapyrrole synthesis
21 redox
26 miscellaneous
27 RNA
29 protein
34 transport
35 not assigned
E
HSFA2 (II-4)
GLK1 (II-6)
BBX15 (II-4)
WRKY40 (III-9)
Normalized count
1. FMT/clpc1-1
2. clpc1-1
3. fmtclpc1-1
4. Wt
5. fmt
* <0.05
** < 0.01
*** < 0.001
****< 0.0001

Fig. 5A-E

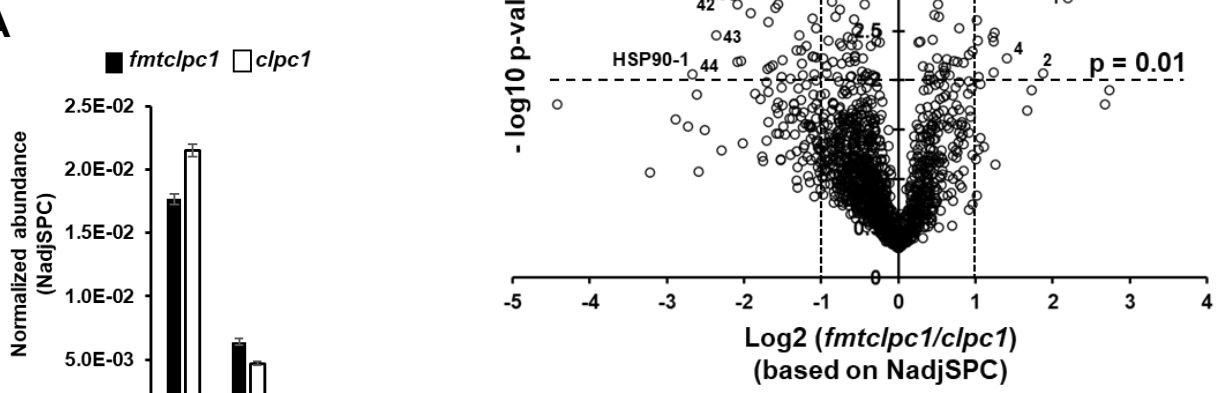

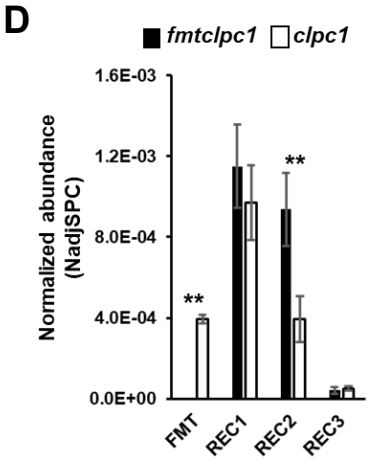

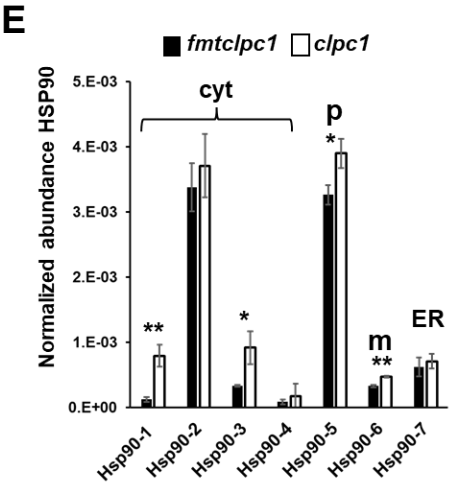

C **Differentially accumulating proteins (p<0.01; 0.5<x>2) based on NadjSPC in *clpc1* vs *fmt clpc1*.**

Accession	#	Name	Location (a)	*fmtclpc1/clpc1* (b)	p value
AT4G27585.1	1	Stomatin-like 1 (SPL1)	m	4.587	0.001
ATCG01100.1	2	NDH A (NDH-1)	p-t	3.679	0.009
AT5G58270.1	3	AMT3 transporter of GSSG	m	3.085	0.001
AT5G47110.1	4	Lil3.1	p-t	2.654	0.006
AT3G47930.1	5	galactono-1,4-lactone dehydrogenase (GLDH)	m	2.373	0.003
AT4G25080.1	6	magnesium-protoporphyrin IX methyltransferase	p-t	2.351	0.000
AT1G44575.1	7	psbS	p-t	2.344	0.004
AT4G28080.1	8	reduced chloroplast coverage 2(REC2)	cyt	2.342	0.008
AT1G77090.1	9	OEC23-like-5 (TL29.8)	p-t	2.324	0.004
AT5G54270.1	10	LHCII-3	p-t	2.064	0.000
AT2G42220.1	11	rhodanese-like domain protein	p-t	2.056	0.009
AT3G08940.2	12	LHCII-4.2 - CP29	p-t	2.033	0.004
AT1G48030.1	13	E3-1 dihydrolipoamide dehydrogenase 1 (MTLPD1)	m	2.025	0.002
AT4G31120.1	14	protein arginine methyltransferase (PRMT5)	n/cyt	0.478	0.006
AT1G63680.1	15	MurE ligase family (TAC)	p	0.475	0.003
AT4G33030.1	16	UDP-sulfoquinovose synthase (SQD1)	p	0.471	0.009
AT1G53210.1	17	sodium/calcium exchanger protein	vac	0.467	0.006
AT1G12770.1	18	DExD box RNA helicase (RH47) (EMB1586)	p	0.462	0.002
AT1G47260.1	19	Carbonic anhydrase - complex I	m	0.461	0.006
AT3G61220.1	20	NADPH short-chain dehydrogenase/reductase (SDR)	cyt	0.438	0.004
AT2G22170.1	21	PLAT2- lipid-associated protein	er/cyt	0.424	0.009
AT5G06600.1	22	ubiquitin-specific protease 12 (UBP12)	n/cyt	0.418	0.007
AT3G14310.1	23	pectin methylesterase	cw	0.418	0.005
AT5G18570.1	24	GTPase Obg A2 (OBG-A2)	p	0.415	0.000
AT1G74850.1	25	pentatricopeptide (PPR) repeat (pTAC2)	p	0.410	0.000
AT1G77590.1	26	acyl-CoA synthetase (LACS9)	p	0.410	0.003
AT3G06430.1	27	PPR2- PPR protein - interacts with 23S RNA	p	0.399	0.005
AT5G37600.1	28	glutamine synthetase (GS1)	cyt	0.352	0.006
AT3G61260.1	29	remorin protein	pm	0.349	0.009
AT5G65720.1	30	NFS1 or AtMtNIFS	m	0.338	0.002
AT5G05200.1	31	ABC1 kinase 9 (ABC1K9)	p	0.330	0.002
AT4G39540.1	32	shikimate kinase	p (likely)	0.324	0.007
AT1G04850.1	33	ubiquitin-associated (UBA)	not p	0.316	0.007
AT3G28290.1	34	integrin-related protein 14a	pm/cyt	0.311	0.003
AT2G20020.1	35	CAF1 - splice factor group II intron	p	0.308	0.008
AT1G78510.1	36	solanesyl diphosphate synthase 1 (SPS1) - PQ9/PC8 synthesis	p	0.276	0.001
AT3G22120.1	37	Cell wall plasma membrane linker protein (CWLP)	cw	0.266	0.002
AT2G32520.1	38	dienelactone hydrolase	not p	0.242	0.006
AT2G26900.1	39	pyruvate importer (BASS2)	p	0.236	0.002
AT2G29530.1	40	Translocase inner membrane subunit 10 (TIM10)	m	0.235	0.007
AT3G02060.1	41	DEAD/DEAH box helicase	p	0.226	0.001
AT1G30120.1	42	Plastidial Pyruvate Dehydrogenase E1 -beta subunit	p	0.205	0.001
AT4G14690.1	43	Lil1.2 - Elip2	p-t	0.194	0.004
AT5G52640.1	44	HSP90-1 (HSP81/83)	cyt	0.157	0.009
AT3G52140.1	45	FRIENDLY (related to REC1,2,3)	cyt	0.060	0.000

(a) p = plastid, p-t = plastid-thylakoid, m = mitochondria, cyt = cytosol, vac = vacuole, pm = plasma membrane, er = endoplasmic reticulum, n = nucleus, cw = cell wall
(b) relative abundance ratio for *fmtclpc1/clpc1* based on NadjSPC

Fig. 6A-E

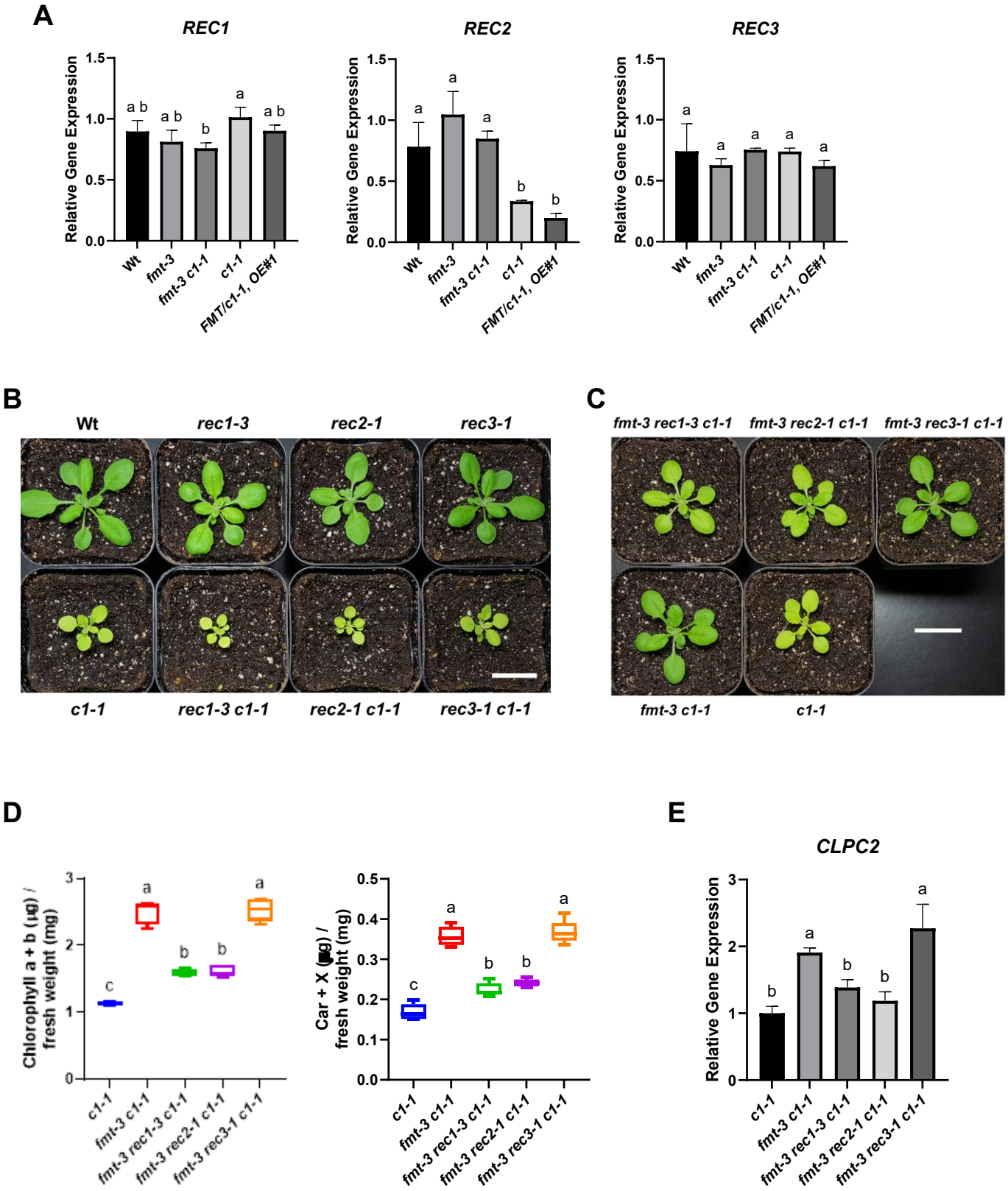
A
REC1
REC2
REC3
Relative Gene Expression
1.5
1.0
0.5
0.0
a b
a b
b
a
a b
a
a
a
b
b
a
a
a
a
a
Wt
fmt-3
fmt-3 c1-1
c1-1
FMT/c1-1, OE#1
B
Wt
rec1-3
rec2-1
rec3-1
c1-1
rec1-3 c1-1
rec2-1 c1-1
rec3-1 c1-1
C
fmt-3 rec1-3 c1-1
fmt-3 rec2-1 c1-1
fmt-3 rec3-1 c1-1
fmt-3 c1-1
c1-1
D
Chlorophyll a + b (µg) / fresh weight (mg)
3
2
1
0
c
a
b
b
a
Car + X (µg) / fresh weight (mg)
0.5
0.4
0.3
0.2
0.1
0.0
c
a
b
b
a
c1-1
fmt-3 c1-1
fmt-3 rec1-3 c1-1
fmt-3 rec2-1 c1-1
fmt-3 rec3-1 c1-1
E
CLPC2
Relative Gene Expression
3
2
1
0
b
a
b
b
a

Fig. 6F-G

F

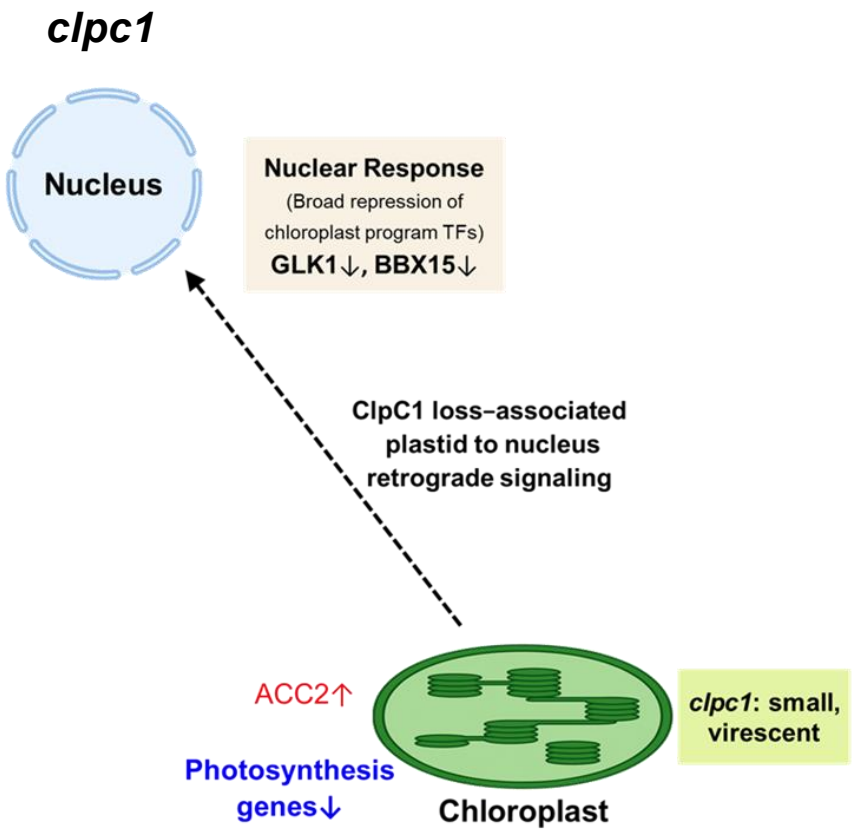
clpc1
Nucleus
Nuclear Response
(Broad repression of chloroplast program TFs)
GLK1↓, BBX15↓
ClpC1 loss-associated plastid to nucleus retrograde signaling
ACC2↑
Photosynthesis genes↓
Chloroplast
clpc1: small, virescent

G

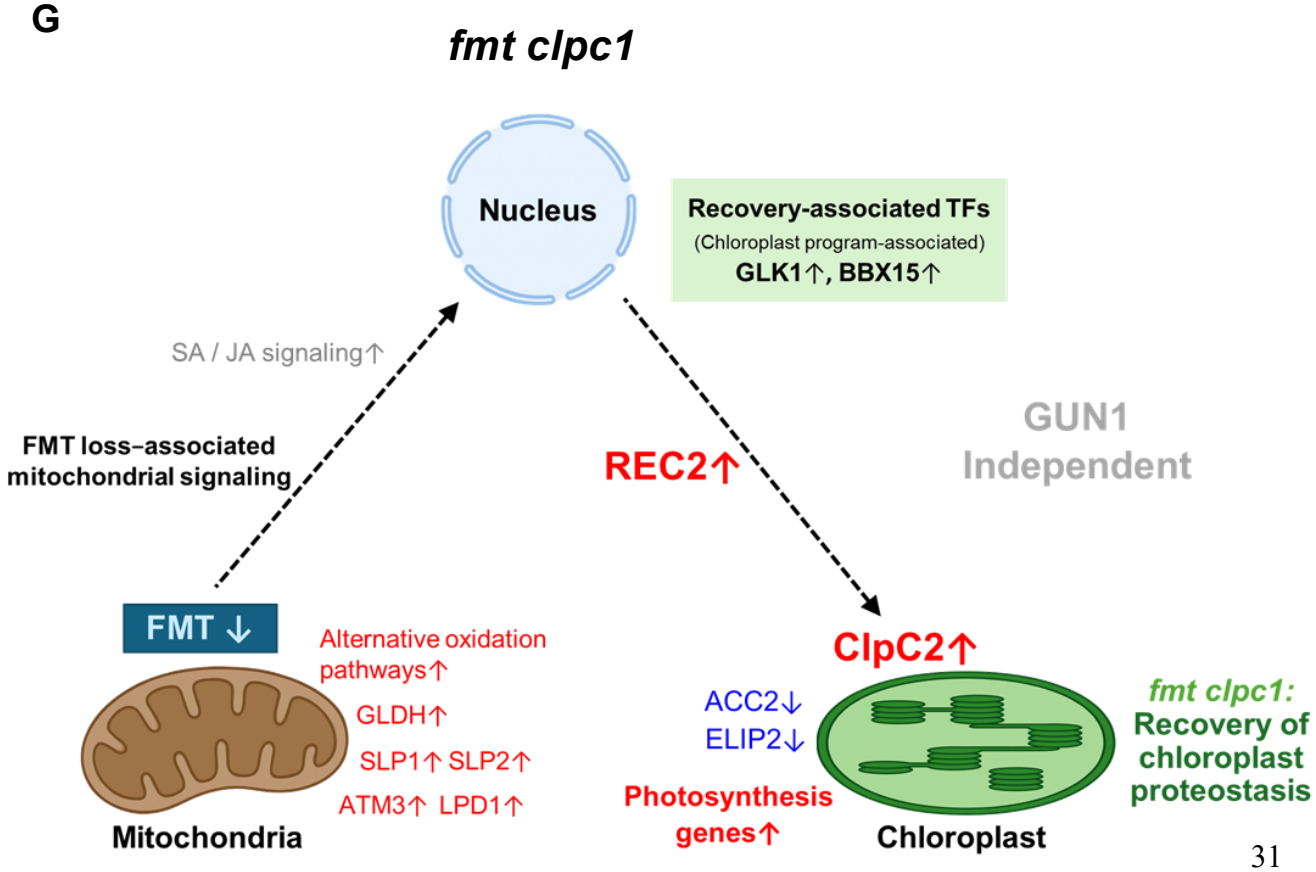
fmt clpc1
Nucleus
Recovery-associated TFs
(Chloroplast program-associated)
GLK1↑, BBX15↑
SA / JA signaling↑
FMT loss-associated mitochondrial signaling
REC2↑
GUN1 Independent
FMT ↓
Alternative oxidation pathways↑
GLDH↑
SLP1↑ SLP2↑
ATM3↑ LPD1↑
Mitochondria
ClpC2↑
ACC2↓
ELIP2↓
Photosynthesis genes↑
Chloroplast
fmt clpc1: Recovery of chloroplast proteostasis

Materials and Methods

EMS Mutagenesis and Suppressor Mapping by Whole-Genome Sequencing

Approximately 10,000 *Arabidopsis thaliana clpc1-1* seeds (Col-0 background) were subjected to ethyl methanesulfonate (EMS) mutagenesis following standard procedures [64]. Treated seeds (M1 generation) were sown on soil and grown under long-day conditions (16/8 hour light/dark cycle at 100 µmol photons m^{-2} s^{-1}, 22 °C). M2 seeds were collected in bulk from individual M1 plants and screened for suppressor phenotypes. The *clpc1-1* mutant exhibits a strong chlorotic and stunted phenotype, allowing visual identification of M2 seedlings with restored leaf greening and improved growth. Approximately 60 groups of M2 seedlings were examined, and ~10 independent suppressor candidates showing partial or near-complete phenotypic recovery were identified. Four lines exhibiting the strongest recovery were selected for further analysis and designated *socc* (*suppressor of clpc1*). Each *socc* line was backcrossed to the parental *clpc1-1* mutant to generate BC1F2 populations. Segregation of the suppressor phenotype among BC1F2 progeny followed an approximate 1:3 ratio (green:chlorotic), consistent with monogenic recessive inheritance.

For bulked segregant analysis, leaf tissue from at least 50 green and 50 chlorotic BC1F2 plants was harvested separately. Genomic DNA was extracted using the DNeasy Plant Mini Kit (Qiagen), and DNA from plants of the same phenotype was pooled to generate "green" and "chlorotic" bulks. Whole-genome sequencing (WGS) was performed by BGI Genomics (Hong Kong). Candidate causal variants were identified by comparing allele frequency differences between the green and chlorotic bulks using the SIMPLE pipeline [65]. Putative causal mutations were further validated by genetic complementation.

Plant Growth, T-DNA Mutant Isolation, and RNA Preparation and RT-PCR Analysis

Plant growth, genotyping, and RNA extraction were performed as described previously [10]. Various growth conditions are detailed in the figure legends. All T-DNA insertion lines were in the Columbia background and are as follows: *FMT* (AT3G52140), SALK_046271 (*fmt-3*) and SALK_056717 (*fmt-4*); *CLPC1* (AT5G50920), SALK_014058 (*clpc1-1*); *CLPC2* (AT3G48870), SAIL_622_B05 (*clpc2-2*); *CLPR2* (AT1G12410), SALK_046378 (*clpr2-1*); *CLPT1* (AT4G25370), GK-285A05 (*clpt1-2*); *CLPT2* (AT4G12060), SAIL_340A10 (*clpt2-1*); *TOC33* (AT1G02280), N2107726 (*ppi1-1*); *TIC40* (AT5G16620), SAIL_92_C10 (*tic40-4*); *GUN1* (AT2G31400), SAIL_33_D01 (*gun1-101*); *REC1* (AT1G01320), SALK_049453C (*rec1-3*); *REC2* (AT4G28080), SALK_020337C (*rec2-1*); and *REC3* (AT1G15290), SAIL_1164_H02 (*rec3-1*).

For RNA-seq analysis, total RNA was isolated using the RNeasy Plant Mini Kit (Qiagen). For RT-PCR, total RNA was isolated using either the RNeasy Plant Mini Kit (Qiagen) or the XENOPURE Total RNA Purification Kit (CelltoBio). First-strand cDNA was synthesized from equal amounts of total RNA using SuperScript III Reverse Transcriptase (Invitrogen) or TOPscript Reverse Transcriptase (Enzynomics). Semi-quantitative RT-PCR and RT-qPCR were performed as

described previously [15,66]. Graphs were generated using GraphPad Prism 10. Primers used for genomic PCR, RT-PCR analysis, and various complementation assays are listed in table S2.

Cloning and Complementation

For *FMT*, the full-length native promoter and 5′UTR of *FMT* (1.0 kb), together with the full-length *FMT* genomic DNA (8.0 kb), totaling 9.0 kb, were PCR-amplified using KOD polymerase (TOYOBO). The PCR products were cloned into a modified pCR8/GW/TOPO vector (Invitrogen), into which BamHI and NotI restriction sites were introduced. Using LR Clonase (Invitrogen), the DNA fragment was transferred into the pGWB4 Gateway destination plant binary vector. For *CLPC2*, the full-length native promoter and 5′UTR of *CLPC2* (1.9 kb), together with the full-length *CLPC2* genomic DNA (5.6 kb), totaling 7.5 kb, were PCR-amplified using KOD polymerase (TOYOBO). The PCR products were cloned into a modified pCR8/GW/TOPO vector (Invitrogen), into which PstI and NotI restriction sites, as well as a StrepII tag and a *nosT* sequence (0.5 kb), were introduced. Using LR Clonase (Invitrogen), the DNA fragment was transferred into the pMDC99 Gateway destination plant binary vector. The primers used are listed in table S2. Competent cells of *Agrobacterium tumefaciens* strain GV3101 were transformed with the binary vectors. Plant transformation and selection were performed as described previously [10], using the *Agrobacterium*-mediated floral dip method with selection on ½ MS agar plates containing 25 µg/mL hygromycin (Duchefa Biochemie). Complemented lines were identified and verified by PCR genotyping.

Generation of Mutant Lines Using CRISPR/Cas9

Mutations in *CLPC1* were generated using the CRISPR/Cas9 system. sgRNAs were designed with CRISPR-P v2.0 and cloned into the pBR-Cas9 vector (provided by Dr. Jae-Young Yun, SeoulTech, Seoul, Korea). *Arabidopsis thaliana* Col-0 plants were transformed by the Agrobacterium-mediated floral dip method (*A. tumefaciens* GV3101). Transgenic plants were screened by PCR amplification of the target region followed by Sanger sequencing of CTAB-extracted DNA. Two independent knockout alleles were recovered: *clpc1-4*, carrying a 1-bp insertion in exon 4, and *clpc1-5*, containing a 32-bp deletion plus a single-nucleotide substitution in the same exon. Both mutations introduce frameshifts predicted to abolish ClpC1 protein function. Cas9-free homozygous segregants were identified by PCR-based genotyping (primer sequences in table S2) and used for all subsequent analyses.

Pigment Analysis

Chlorophyll and carotenoid contents on a fresh-weight basis were measured in 80% acetone as described previously [13].

Photosynthetic Efficiency Analysis

Fv/Fm measurements were performed as described previously [66]. Briefly, plants were dark-adapted for 30 min at room temperature, and chlorophyll fluorescence parameters (Fo and Fm) were recorded using a FluorCam 800MF (Photon Systems Instruments, Czech Republic). Fv/Fm values were calculated as (Fm - Fo)/Fm to evaluate photosystem II photochemical efficiency under normal growth conditions.

Transmission Electron Microscopy (TEM)

Leaves from 23-day-old plants were fixed with a mixture of 2% (v/v) glutaraldehyde and 2% (v/v) paraformaldehyde in 0.05 M cacodylate buffer (pH 7.2) at room temperature for 4 h. The samples were washed with the same buffer and post-fixed with 1% (w/v) OsO_4 in 0.05 M cacodylate buffer at room temperature for 1 h. Fixed samples were washed again with the buffer and dehydrated through a graded ethanol series (30–100%). The samples were then embedded in LR White resin at 50 °C for 24 h. Ultrathin sections (80–100 nm thick) were prepared using an ultramicrotome equipped with a diamond knife. Sections were stained with uranyl acetate and lead citrate and examined using a transmission electron microscope (JEM-2100F, JEOL Ltd., Japan).

Chloroplast Isolation and Total Leaf Protein Extraction

For chloroplast isolation, leaves from wild-type and various mutant alleles were briefly homogenized in grinding medium (50 mM HEPES-KOH, pH 8.0, 330 mM sorbitol, 2 mM EDTA, 5 mM ascorbic acid, 5 mM cysteine, and 0.03% BSA) and filtered through a nylon mesh. The crude plastids were collected by centrifugation at 1,100 g for 2 min and further purified on 35–85% Percoll cushions (Percoll in 0.6% Ficoll and 1.8% polyethylene glycol) by centrifugation at 3,750 g for 10 min, followed by one additional wash in grinding medium lacking ascorbic acid, cysteine, and BSA. Chloroplasts were subsequently lysed in 10 mM HEPES-KOH, pH 8.0, 5 mM $MgCl_2$, and 15% glycerol, containing a mixture of protease inhibitors, under mild mechanical disruption. Protein concentrations were determined using the BCA Protein Assay Kit (Thermo Scientific). Total leaf proteins were extracted as described previously [15].

Immunoblot Analysis

For immunoblotting, proteins were transferred onto nitrocellulose or polyvinylidene fluoride (PVDF) membranes and probed with specific antibodies using chemiluminescence detection, following standard procedures. The antisera against *Arabidopsis* ClpF and ClpS1 were described previously [14]. The anti-PAA2 antibody was kindly provided by Dr. Marinus Pilon (Colorado State Univ., Fort Collins, CO, USA).

PAA2 Degradation Assay

The PAA2 degradation assay was performed as described previously [18] with minor modifications. Briefly, *Arabidopsis thaliana* seedlings were grown on half-strength MS agar plates (pH 5.8) containing 0.6% (w/v) agar and 1% (w/v) sucrose for 21 days under short-day conditions (10/14 hour light/dark cycle at 100 µmol photons m^{-2} s^{-1}). For copper treatments, 5 µM $CuSO_4$ was added to the growth medium, and for control conditions, 0.05 µM $CuSO_4$ was used. Total leaf protein extraction and immunoblot analysis were performed as described previously [15]. PAA2 abundance was detected using affinity-purified anti-PAA2 antibodies (1:1000 dilution).

RNAseq analysis.

RNA analysis was carried out for five genotypes of Arabidopsis seedlings in stage 1.07, with 3 biological replicates. The genotypes are: WT, *clpc1-1*, *fmt-3*, *fmt-3 clpc1-1*, FMT overexpressed line OE#1 in *clpc1-1* (*FMT/clpc1*). Total RNA was isolated with an RNeasy plant mini kit (Qiagen). Total RNA samples were processed for library preparation and sequencing following the manufacturer's protocol. Briefly, mRNA was enriched from total RNA using oligo(dT) beads targeting the poly(A) tails. The isolated mRNA was then fragmented into smaller pieces, which served as templates for first-strand cDNA synthesis using random primers. Subsequently, second-strand cDNA synthesis was performed, incorporating dUTP in place of dTTP to enable strand specificity. The resulting double-stranded cDNA underwent end-repair and 3′-adenylation, after which sequencing adapters were ligated. The adapter-ligated fragments were then amplified via PCR, and the amplified libraries were subjected to quality control assessment. Following quality control, the libraries were circularized and further amplified to form DNA nanoballs (DNBs). Finally, sequencing was performed using the DNBSEQ platform (DNBSEQ Technology). Raw data with adapter sequences or low-quality sequences was filtered using SOAPnuke [67]. For individual replicate-level expression analyses, the HISAT2 aligned bam files were used for reads counting using the featureCounts program [68]

Data normalization (Supplementary Data Set 1A), downstream analysis of differentially expressed genes, and adjusted p-value calculation were performed using the DESeq2 package v.1.44.0 [69] in R v4.4.3. . Specifically, a DESeqDataSet object was generated using the raw counts, with design = ~genotype. Pairwise results for each genotypic comparison of interest were then generated using the 'results()' function of DESeq2, with the function's contrast parameter being used to specify the relevant genotypes. The p-values were determined by the default Wald test, and these p-values were adjusted using the Benjamini-Hochberg method. Genes with a differential expression of at least two-fold ($x<0.5$ or $x>2$) and adjusted p value <0.01 in one of the 10 possible comparisons across genotypes were considered for further investigation. This resulted in a set of 4745 nuclear protein-coding genes that we annotated for subcellular protein location (in particular chloroplast and mitochondria) and function (using the MapMan bin system) from public resources (TAIR, PPDB and publications) (Supplementary Data Set 1B). The gene clustering was generated using the Ward D2 method with Euclidean distance in the pheatmap v1.0.13 R package (Supplementary Data Set 1B). PCA analysis was performed using the GLEE software [13]. The graphs are generated either using Microsoft Excel or GraphPad Prism 10.

Comparative Proteome Analysis

Total proteome extracts of seedlings of *clpc1-1* and *fmt-3 clpc1-1* (each with three biological replicates) were separated by Tris-Glycine SDS-PAGE using 8-16% precast gels (Cat. No. KG7550-BC; KOMA Biotech, Korea). Gels were stained with Coomassie Brilliant Blue. Each of the six SDS-PAGE gel lanes was completely cut into consecutive gel slices (10 slices per lane), followed by reduction, alkylation, and in-gel digestion with trypsin as described in [70]. The extracted peptides were resuspended in 2% formic acid and analyzed using a QExactive mass spectrometer equipped with a nanospray flex ion source and interfaced with a nanoLC system and autosampler (Dionex Ultimate 3000 Binary RSLCnano system) as described in [19] with the exception that AGC target values were set at 1 x 10^6 for the MS survey scans and maximum scan time 30 ms and 5.10^5 for MSMS scans and maximum scan time 50 ms [Other parameters: MS: 70k resolution, scan range 400-2000 m/z; MSMS: 17.5k resolution, top10, loop count 10, isolation window 2.0 m/z, dynamic exclusion 15 sec].

Peak lists in MGF format were generated from RAW files using Distiller software (version 2.7.1.0) in default mode (Matrix Science). MGF files were searched with MASCOT v2.4.0 against TAIR10 including a set of typical contaminants and the decoy (71148 sequences; 29099536 residues). Two parallel searches (Mascot p-value <0.01 for individual ion scores; precursor ion window 700 to 3500 Da) were carried out: (i) Full tryptic (error tolerance 10 ppm for MS and 0.5 Da for MS/MS) and (ii) Semi-tryptic (error tolerance 6 ppm and 0.5 Da for MS/MS) in both cases with fixed Cys-carbamido-methylation and variable M-oxidation, N-terminal acetylation, N-terminal formylation and 2 missed cleavages (in Mascot PR or PK does not count as missed cleavage). In-house post-Mascot filtering removed redundancies between the full and semi-tryptic searches and removed spectral matches with ion scores below 33. Proteins could only be identified by the spectral counting method (SPC) with the full tryptic (6 ppm) search. The semi-tryptic search served to increase protein coverage and was combined with the full tryptic search results. Final false discovery rate for proteins identified with one spectral match was zero for those with two or more spectral matches. Proteins identified by MS/MS spectra that were all shared with other proteins identified by unique peptides were discarded.

Proteins were quantified by the spectral counting method (SPC) using full and semi-tryptic peptides search results. For quantification by spectral counting, each accession was scored for total spectral counts (SPC), unique SPC (uniquely matching to an accession) and adjusted SPC [70]. The latter assigns shared peptides to accessions in proportion to their relative abundance using unique spectral counts for each accession as a basis. Proteins that shared more than 80% of their matched peptides with other proteins across the complete dataset were grouped into families quantified as groups with these homologs [70]. After selecting only the best scoring isoform model per protein, proteins that shared a significant number of matched spectra were grouped, and proteins and groups with less than 3 adjSPC were discarded for further analysis; this resulted in 2976 proteins including 124 groups. For significance analysis and Volcano plots to compare the two genotypes, the minimal total adjSPC was raised to >12, resulting in 1529 proteins and groups; this ensured a more robust dataset and lower FDR. Within each sample, a value of 0.99 AdjSPC was imputed for all proteins with missing values. This was followed by normalization of the adjSPC to the total adjSPC of the samples resulting in NadjSPC for each protein. Average NadjSPC per genotype across the 3 replicates were calculated and *fmt1clpc1/clpc1* NadjSPC ratios were determined for each protein. p-value and q-value (FDR) were then calculated to determine proteins that showed

significant abundance differences between *clpc1* and *fmtclpc1*. We created Volcano plots and plotted total protein abundance against the protein abundance ratios.